Intelligent Reflecting Surface Based Passive Information Transmission: A Symbol-Level Precoding Approach

Rang Liu, *Graduate Student Member, IEEE*, Ming Li, *Senior Member, IEEE*, Qian Liu, *Member, IEEE*, A. Lee Swindlehurst, *Fellow, IEEE*, and Qingqing Wu, *Member, IEEE*

***Abstract*—Intelligent reflecting surfaces (IRS) have been proposed as a revolutionary technology owing to its capability of adaptively reconfiguring the propagation environment in a cost-effective and hardware-efficient fashion. While the application of IRS as a passive reflector to enhance the performance of wireless communications has been widely investigated in the literature, using IRS as a passive transmitter recently is emerging as a new concept and attracting steadily growing interest. In this paper, we propose two novel IRS-based passive information transmission systems using advanced symbol-level precoding. One is a standalone passive information transmission system, where the IRS operates as a passive transmitter serving multiple receivers by adjusting its elements to reflect unmodulated carrier signals. The other is a joint passive reflection and information transmission system, where the IRS not only enhances transmissions for multiple primary information receivers (PIRs) by passive reflection, but also simultaneously delivers additional information to a secondary information receiver (SIR) by embedding its information into the primary signals at the symbol level. Two typical optimization problems, i.e., power minimization and quality-of-service (QoS) balancing, are investigated for the proposed IRS-based passive information transmission systems. Simulation results demonstrate the feasibility of IRS-based passive information transmission and the effectiveness of our proposed algorithms, as compared to other benchmark schemes.**

***Index Terms*—Intelligent reflecting surface (IRS), symbol-level precoding, passive information transmission, passive beamforming.**

Manuscript received January 24, 2021; revised April 12, 2021; accepted May 12, 2021. Date of publication May 19, 2021; date of current version July 20, 2021. This work was supported in part by the National Natural Science Foundation of China under Grants 61971088, 62071083, U1808206, and U1908214, in part by the Natural Science Foundation of Liaoning Province under Grant 2020-MS-108, in part by the Fundamental Research Funds for the Central Universities under Grant DUT20GJ214, in part by the Dalian Science and Technology Innovation Project under Grant 2020JJ25CY001, in part by the Open Research Fund of National Mobile Communications Research Laboratory, Southeast University under Grants 2021D08 and 2021D15, in part by the U.S. National Science Foundation under Grants ECCS-2030029 and CCF-2008714, in part by the Guangdong NSF under Grant 2021A1515011900, and in part by FDCT 0108/2020/A. The review of this article was coordinated by Dr. Chau Yuen. (*Corresponding Author: Ming Li.*)

Rang Liu is with the School of Information and Communication Engineering, Dalian University of Technology, Dalian 116024, China (e-mail: liurang@mail.dlut.edu.cn).

Ming Li is with the School of Information and Communication Engineering, Dalian University of Technology, Dalian 116024, China, and also with the National Mobile Communications Research Laboratory, Southeast University, Nanjing 210096, China (e-mail: mli@dlut.edu.cn).

Qian Liu is with the School of Computer Science and Technology, Dalian University of Technology, Dalian 116024, China (e-mail: qianliu@dlut.edu.cn).

A. Lee Swindlehurst is with the Center for Pervasive Communications and Computing, University of California, Irvine, CA 92697 USA (e-mail: swindle@uci.edu).

Qingqing Wu is with the State Key Laboratory of Internet of Things for Smart City, University of Macau, Macau 999078, China, and also with the National Mobile Communications Research Laboratory, Southeast University, Nanjing 210096, China (e-mail: qingqingwu@um.edu.mo).

Digital Object Identifier 10.1109/TVT.2021.3081773

I. Introduction

During the past decade, various techniques have been developed to accommodate the rapidly increasing demands for high data rates and diverse quality-of-service (QoS). Massive multi-input multi-output (MIMO), millimeter wave (mmWave) communication, and ultra-dense networks are three representative approaches for enhancing wireless network performance [1]. However, the required high hardware cost as well as the resulting increased energy consumption remain as roadblocks in their practical implementation. As a energy/spectrum/hardware-efficient solution for future wireless networks, intelligent reflecting surfaces (IRS) have attracted abundant attention owing to their ability to tailor the radio environment in a cost-effective and hardware-efficient fashion [2]-[9].

An IRS is a man-made two-dimensional (2D) surface composed of a large number of reconfigurable passive elements. Each element can independently manipulate the phase of the incident signals in a real-time programmable manner, thus collaboratively enabling adaptive reflection beamforming in three-dimensional (3D) space. By intelligently controlling the signal reflection, an IRS can create a more favorable propagation environment, which used to be more or less out of the control of the system designer. Furthermore, the reflection beamforming offers additional degrees of freedom (DoFs) for addressing severe channel fading and refining channel statistics. Therefore, IRS is attracting steadily growing interest in both academia and industry. In the past several years, researchers have devoted substantial efforts to exploring the potential of IRS as a passive relay/reflector to greatly expand coverage, improve transmission quality, and assure security, [10]-[18], etc. By judiciously designing the IRS phase-shifts, the signals reflected by the IRS and from other paths can coherently add up at intended receivers and/or cancel out at unintended receivers to improve system performance. Various advanced optimization algorithms and deep learning-based methods [19], [20] have been proposed for

the designs of IRS-assisted systems. In addition, IRS have also found some novel applications in holographic MIMO [21], [22], mobile edge computing, sensing and localization, etc. [5], [8].

In most of the applications mentioned above, the IRS is deployed as a *passive reflector* to enhance performance by adaptively reflecting the incident signals, which are already modulated/precoded by an active transmitter. Meanwhile, the novel concept of utilizing IRS as *passive transmitters* was presented in [3], where the IRS changes the parameters of the reflecting elements to modulate and transmit information symbols by exploiting an unmodulated carrier signal generated by a nearby radio-frequency (RF) signal generator. Testbed platforms utilizing IRS to realize a quadrature phase-shift-keying (QPSK) transmitter [23] and 8-PSK transmitter [24] have validated this idea. In particular, the IRS-based passive transmitter can realize virtual MIMO communication with only one RF chain and very cost-effective reflecting elements at the transmitter side, which thus makes it very promising for practical wireless networks due to the significantly reduced hardware complexity and energy consumption. While IRS-based single-stream transmitters have been investigated in [3], [23], [24], exploiting IRS to simultaneously transmit multiple data streams and serve multiple users has not been studied yet, which thus motivates this work.

In addition, there has been growing interest in combining the passive reflection and passive transmission capabilities of IRS. In these joint applications, besides enhancing the quality of the primary signals using the IRS, one can also modulate and embed the secondary information into the primary signals by appropriately varying the IRS reflection coefficients. Such an IRS-based symbiotic radio system achieves higher spectrum efficiency by exploiting the same spectrum resource for both the primary and secondary information transmissions. Compared with conventional ambient backscatter-based symbiotic radio systems [25], [26], where the backscatter device usually has only a single-antenna, the abundant reflecting elements of the IRS provide more DoFs to combat the double fading effect and thus enhance the quality of the information transmissions. Specifically, in [27], [28], the authors presented a joint passive beamforming and information transfer system in which the secondary information is modulated by the on/off states of the IRS reflecting elements. In [29], the authors proposed a reflecting modulation scheme for an IRS-based passive transmitter. In [30], the IRS operates as an Internet-of-Things (IoT) device to transfer secondary information by jointly designing the active beamforming and passive reflecting. While these works [3], [23], [24], [27]-[32] explored the feasibility of using an IRS as a passive transmitter, the selection of reflection patterns are limited for the secondary information transmission, e.g., only two antipodal reflection patterns were considered in [30]. Therefore, the full potential of IRS has not been exploited in these works. More importantly, in these existing designs, both primary and secondary receivers need to jointly detect the primary and secondary information symbols, which causes high computational complexity to the receivers. Furthermore, the more complicated case with passive information transmission to multiple receivers has not been investigated yet, which motivates us to develop this work.

We note that in IRS-based passive transmission schemes, each information symbol is modulated by varying the reflecting elements of the IRS, which is similar to the mechanism employed in symbol-level precoding [33]-[36]. In symbol-level precoding, the multi-antenna transmitter varies its precoder in a symbol-by-symbol fashion to turn the harmful multi-user interference (MUI) into constructive and beneficial signals. Such methods can exploit both the spatial and symbol-level DoFs to significantly improve the symbol error-rate (SER) performance of multiuser systems. Moreover, the receivers in the symbol-level precoding system can demodulate information using a simple hard-decision rule since the optimizations at the transmitter side consider the specific modulation type known at the receiver. In addition, with current semiconductor technologies, fast positive-intrinsic-negative (PIN) or Schottky diodes can realize switching within nanoseconds [37]. Existing testbed platforms [23], [24] have also validated the feasibility of adjusting IRS at symbol-level speeds. Inspired by these findings, in this paper we show how to realize IRS-based passive information transmissions by exploiting symbol-level precoding technology, which provides symbiotic benefits from various aspects. The main contributions in this paper are summarized as follows:

- Unlike our previous work [11] on joint symbol-level precoding and IRS passive reflection design, in this paper we use symbol-level precoding to implement IRS-based passive information transmissions in the downlink of a multi-user multi-input single-output (MU-MISO) system. This new symbol-level precoding approach not only fully exploits the DoFs available from the massive number of IRS reflecting elements to enhance the quality of information transmissions, but also allows the receivers to employ a very simple symbol detector, thus rendering itself particularly appealing in practical implementation.
- For the case where the IRS works as a standalone passive transmitter to deliver information to multiple single-antenna users, we design the IRS phase-shifts to minimize the transmit power subject to a given set of QoS requirements. Efficient algorithms based on Riemannian manifold optimization and the branch-and-bound algorithm are proposed to obtain continuous/high-resolution phase-shifts and low-resolution quantized phase-shifts, respectively. We also investigate the QoS balancing problem for a given transmit power budget.
- For the case where the IRS works as a joint passive reflector and transmitter, also known as a symbiotic radio system, the IRS enhances the primary information transmissions from the multi-antenna base station (BS) to multiple single-antenna users, and simultaneously delivers secondary information to one additional user by embedding the secondary information into the primary signals. The power minimization and QoS balancing problems are also investigated by iteratively solving for the precoders and reflectors using efficient gradient projection-based and conjugate gradient-based algorithms.

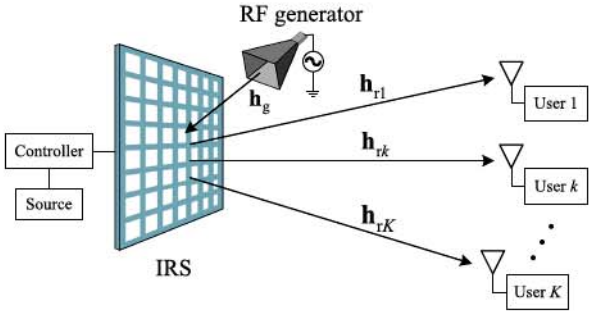

Fig. 1. An IRS-based MU-MISO passive information transmission system.

- Finally, we provide extensive simulation results to demonstrate the feasibility of exploiting symbol-level precoding for passive information transmissions in IRS-based MU-MISO systems, and to illustrate the effectiveness of our proposed algorithms.

Notation: Boldface lower-case and upper-case letters indicate column vectors and matrices, respectively. $(\cdot)^T$ and $(\cdot)^H$ denote the transpose and the transpose-conjugate operations, respectively. $\mathbb{C}$ denotes the set of complex numbers. $|a|$ and $\|\mathrm{a}\|$ are the magnitude of a scalar a and the norm of a vector a, respectively. $y = f\langle x\rangle$ denotes that y is a function of x. $\angle a$ is the angle of complex-valued a. $\Re\{\cdot\}$ and $\Im\{\cdot\}$ denote the real and imaginary part of a complex number, respectively. $\mathrm{diag}\{\mathrm{a}\}$ indicates a diagonal matrix whose diagonal terms are the elements of a. $\mathbf{A}(i,j)$ denotes the element of the i-th row and the j-th column of matrix $\mathbf{A}$, and $\mathrm{a}(i)$ denotes the i-th element of vector a.

II. Passive Information Transmission System

A. System Model

Consider an MU-MISO system as shown in Fig. 1, where the IRS equipped with N reflecting elements simultaneously serves K single-antenna users. Specifically, using the idea of symbol-level precoding, the IRS modulates the information symbols onto the high-frequency carrier signals (generated from a nearby RF signal generator) by adjusting its reflection coefficients. Since the information modulation and precoding are implemented at the IRS side, which only has passive components, we refer to this communication system as a passive information transmission system. As discussed in [3] and [31], the RF generator is sufficiently close to the IRS and utilizes a horn antenna to focus the signals on the IRS. Therefore, the RF generator and IRS can be seen as a transmitter with only one RF chain and multiple reflecting elements, which realizes a virtual MIMO communication with significantly reduced hardware complexity and cost. Denote $\boldsymbol{\theta} \in \mathbb{C}^N$ as the vector containing the IRS reflection coefficients. The received baseband signal at the k-th user can be written as[1]

$$r_k = \sqrt{P}\mathrm{h}_{\mathrm{r}k}^H \boldsymbol{\Theta} \mathrm{h}_{\mathrm{g}} + n_k, \tag{1}$$

where P is the transmit power of the RF generator, $\boldsymbol{\Theta} \triangleq \mathrm{diag}\{\boldsymbol{\theta}\}$, $\mathrm{h}_{\mathrm{r}k} \in \mathbb{C}^N$ is the channel vector from the IRS to the k-th user, h_{g} is the channel vector from the RF generator to the IRS, and $n_k \sim \mathcal{CN}(0, \sigma^2)$ is additive white Gaussian noise (AWGN) at the k-th user. Given the availability of various channel estimation approaches [8], [38]-[42], perfect channel state information (CSI) is assumed to be available at the IRS. For simplicity, we denote the equivalent channel from the IRS to the k-th user as $\mathrm{h}_k^H \triangleq \mathrm{h}_{\mathrm{r}k}^H \mathrm{diag}\{\mathrm{h}_{\mathrm{g}}\}$. Then, the received signal for the k-th user can be rewritten as

$$r_k = \sqrt{P}\mathrm{h}_k^H \boldsymbol{\theta} + n_k. \tag{2}$$

To realize passive information transmissions, the IRS modulates the symbols by changing the reflection vector $\boldsymbol{\theta}$ according to the symbols to be transmitted [3]. We assume that the desired symbols for all users are independently Ω-PSK modulated.[2] As a result, there are Ω^K possible combinations of symbols that could be transmitted to the K users. We let $\mathrm{s}_m \triangleq [s_{m,1}, \ldots, s_{m,K}]^T$ for $m = 1, \ldots, \Omega^K$ represent all of the possible symbol vectors. To transmit s_m, an appropriate phase vector $\boldsymbol{\theta}_m$ must be designed, so that the received signal at the k-th user

$$r_{m,k} = \sqrt{P}\mathrm{h}_k^H \boldsymbol{\theta}_m + n_k \tag{3}$$

can be properly decoded according to the pre-known constellation information. In the sequel, we will design the non-linear mapping from s_m to $\boldsymbol{\theta}_m$ using constructive symbol-level precoding [33]-[36]. Considering the ideal reflection model with unit-modulus and continuous phase shifts, each reflecting element should satisfy $|\boldsymbol{\theta}_m(n)| = 1, \forall m, n$.

Using knowledge of the symbol vector s_m to be transmitted, constructive interference (CI) symbol-level precoding converts the MUI into constructive components that push the received noise-free signals away from their corresponding decision boundaries, which greatly improves the detection performance. Thus, the Euclidean distance between the received noise-free signal and its corresponding closest decision boundary is adopted as the metric to measure the users' QoS. More detailed and comprehensive descriptions about constructive interference and symbol-level precoding can be found in [33]-[36]. In order to explicitly demonstrate this metric, we take QPSK modulated symbols as an example, as shown in Fig. 2. Specifically, we assume $s_{m,k} = e^{\jmath\pi/4}$ is the desired symbol of the k-th user, the positive halves of the x and y axes are the decision boundaries for $s_{m,k}$, the shaded green area is its decision region (i.e., CI region), $\overrightarrow{OC} = \sqrt{P}\mathrm{h}_k^H \boldsymbol{\theta}_m$ is the received noise-free signal, $\psi = \pi/\Omega = \pi/4$ is the half angle of the decision region, and $|\overrightarrow{CD}|$ is the Euclidean distance between point C and the corresponding nearest decision boundary. We see that $s_{m,k}$ can be correctly detected at the k-th user when the received signal $r_{m,k}$ lies in the green region. In order to improve the robustness to noise, the phase vector $\boldsymbol{\theta}_m$ should be designed to render the received noise-free signal $\overrightarrow{OC}$ as far away from its decision boundaries

[1]The direct link between the RF generator and the users is ignored since the pure RF signal does not contain information (i.e., a constant baseband value) and can be easily removed at the users. Besides, the RF generator mainly beams the energy towards the IRS rather than the randomly distributed users.

[2]It is noted that symbol-level precoding is related to the modulation type. The designs throughout this paper focus on PSK modulations. The designs for quadrature amplitude modulation (QAM) are left for our future work.

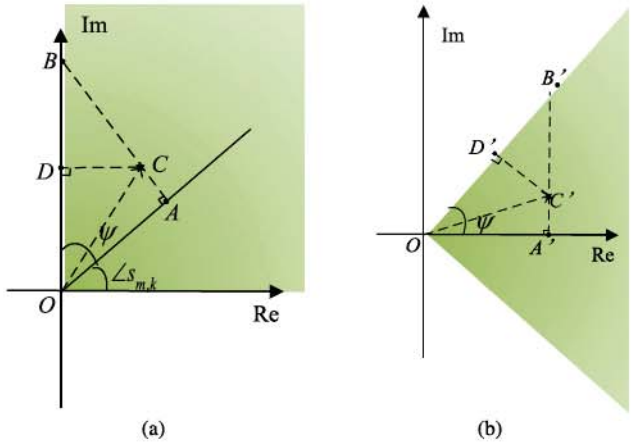

Fig. 2. Symbol-level precoding design for QPSK signals.

as possible. Therefore, $|\overrightarrow{CD}|$ is usually used as the metric to evaluate the QoS of communication since it determines the SER performance. To derive an expression for $|\overrightarrow{CD}|$, we rotate the diagram clockwise by $\angle s_{m,k}$ degrees as shown in Fig. 2(b), where

$$\overrightarrow{OC'} = \widetilde{r}_{m,k} = \sqrt{P}\mathbf{h}_k^H \boldsymbol{\theta}_m e^{-\jmath \angle s_{m,k}}. \tag{4}$$

Then, the Euclidean distance to evaluate the QoS of communication is given by

$$\begin{aligned} \left|\overrightarrow{C'D'}\right| &= \left|\overrightarrow{C'B'}\right| \cos\psi = \left[\left|\overrightarrow{A'B'}\right| - \left|\overrightarrow{A'C'}\right|\right] \cos\psi \\ &= \left[\Re\left\{\overrightarrow{OC'}\right\} \tan\psi - \left|\Im\left\{\overrightarrow{OC'}\right\}\right|\right] \cos\psi \\ &= \Re\left\{\widetilde{r}_{m,k}\right\} \sin\psi - \left|\Im\left\{\widetilde{r}_{m,k}\right\}\right| \cos\psi. \end{aligned} \tag{5}$$

The QoS constraint can thus be expressed as

$$\Re\left\{\widetilde{r}_{m,k}\right\} \sin\psi - \left|\Im\left\{\widetilde{r}_{m,k}\right\}\right| \cos\psi \geq \alpha_k, \ \forall m, k, \tag{6}$$

where α_k is the preset QoS requirement for the k-th user.

B. Design for Power Minimization

In this subsection, we investigate the power minimization problem, which aims to minimize transmit power at the RF generator while satisfying the QoS requirements of all users. Accordingly, the optimization problem is formulated as

$$\min_{\boldsymbol{\theta}_m, \forall m, P} \ P \tag{7a}$$

$$\text{s.t.} \ \ \Re\left\{\widetilde{r}_{m,k}\right\} \sin\psi - \left|\Im\left\{\widetilde{r}_{m,k}\right\}\right| \cos\psi \geq \alpha_k, \ \forall m, k, \tag{7b}$$

$$\widetilde{r}_{m,k} = \sqrt{P}\mathbf{h}_k^H \boldsymbol{\theta}_m e^{-\jmath \angle s_{m,k}}, \ \forall m, k, \tag{7c}$$

$$|\boldsymbol{\theta}_m(n)| = 1, \ \forall m, n. \tag{7d}$$

It can be observed that unlike the constant envelope symbol-level precoding approach in [35], we utilize the IRS to realize passive beamforming and simultaneously consider all possible precoders in one channel coherence time. To efficiently solve this non-convex multivariate optimization problem, we propose to convert it into a univariate problem, which facilitates development of an efficient algorithm.

First, after dividing both sides of the QoS constraint (7b) by $\alpha_k\sqrt{P}$, we have

$$\frac{1}{\sqrt{P}} \leq \frac{1}{\alpha_k}\left[\Re\left\{\widehat{r}_{m,k}\right\} \sin\psi - \left|\Im\left\{\widehat{r}_{m,k}\right\}\right| \cos\psi\right], \ \forall m, k, \tag{8}$$

where $\widehat{r}_{m,k} \triangleq \mathbf{h}_k^H \boldsymbol{\theta}_m e^{-\jmath \angle s_{m,k}}$. By introducing an auxiliary variable $t \triangleq \frac{1}{\sqrt{P}}$, the power minimization problem (7) can be converted to

$$\max_{\boldsymbol{\theta}_m, \forall m, t} \ t \tag{9a}$$

$$\text{s.t.} \ \ t \leq \frac{1}{\alpha_k}\left[\Re\left\{\widehat{r}_{m,k}\right\} \sin\psi - \left|\Im\left\{\widehat{r}_{m,k}\right\}\right| \cos\psi\right], \ \forall m, k, \tag{9b}$$

$$\widehat{r}_{m,k} = \mathbf{h}_k^H \boldsymbol{\theta}_m e^{-\jmath \angle s_{m,k}}, \ \forall m, k, \tag{9c}$$

$$|\boldsymbol{\theta}_m(n)| = 1, \ \forall m, n. \tag{9d}$$

The optimization problem (9) can be further equivalently rewritten as a max-min problem as

$$\max_{\boldsymbol{\theta}_m, \forall m} \ \min_{m,k} \ \frac{1}{\alpha_k}\left[\Re\left\{\widehat{r}_{m,k}\right\} \sin\psi - \left|\Im\left\{\widehat{r}_{m,k}\right\}\right| \cos\psi\right] \tag{10a}$$

$$\text{s.t.} \quad \widehat{r}_{m,k} = \mathbf{h}_k^H \boldsymbol{\theta}_m e^{-\jmath \angle s_{m,k}}, \ \forall m, k, \tag{10b}$$

$$|\boldsymbol{\theta}_m(n)| = 1, \ \forall m, n. \tag{10c}$$

Obviously, problem (10) is also difficult to solve, not only because of the large number of variables, but also the non-differentiable absolute and minimum value functions in the objective (10a), and the non-convex unit-modulus constraint (10c) of the IRS. In the following, we propose to divide the large-scale optimization problem into several sub-problems. For each sub-problem, an approximate differentiable objective is derived, and the non-convex constraint is tackled using a manifold-based algorithm.

Since the optimization of (10) for different $\boldsymbol{\theta}_m, m = 1, \ldots, \Omega^K$, is independent with respect to m, we can equivalently divide this large-scale problem into Ω^K sub-problems. The m-th sub-problem is rewritten as

$$\min_{\boldsymbol{\theta}_m} \ \max_i \ |\Im\{\mathbf{a}_i^H \boldsymbol{\theta}_m\}| \cos\psi - \Re\{\mathbf{a}_i^H \boldsymbol{\theta}_m\} \sin\psi \tag{11a}$$

$$\text{s.t.} \ \ |\boldsymbol{\theta}_m(n)| = 1, \ \forall n, \tag{11b}$$

where $\mathbf{a}_i^H \triangleq \frac{1}{\alpha_k}\mathbf{h}_k^H e^{-\jmath \angle s_{m,k}}, i = K(m-1)+k$. Then, in order to remove the absolute value function and form a more concise objective function, we utilize the property that $|x| = \max\{x, -x\}$ for a scalar x together with some basic linear algebra laws to re-formulate the objective (11a) as

$$|\Im\{\mathbf{a}_i^H \boldsymbol{\theta}_m\}| \cos\psi - \Re\{\mathbf{a}_i^H \boldsymbol{\theta}_m\} \sin\psi = \max\{f_i, g_i\}, \tag{12}$$

where f_i and g_i are defined as

$$f_i \triangleq \Im\{\mathbf{a}_i^H \boldsymbol{\theta}_m\} \cos\psi - \Re\{\mathbf{a}_i^H \boldsymbol{\theta}_m\} \sin\psi = \Re\{\mathbf{b}_i^H \boldsymbol{\theta}_m\}, \ \forall i, \tag{13a}$$

$$g_i \triangleq -\Im\{\mathbf{a}_i^H \boldsymbol{\theta}_m\} \cos\psi - \Re\{\mathbf{a}_i^H \boldsymbol{\theta}_m\} \sin\psi = \Re\{\mathbf{c}_i^H \boldsymbol{\theta}_m\} \ \forall i. \tag{13b}$$

For notational conciseness in the following algorithm development, in (13a) and (13b), we have defined

$$\mathbf{b}_i^H \triangleq -\mathbf{a}_i^H \sin\psi + \mathbf{a}_i^H e^{-\jmath\frac{\pi}{2}} \cos\psi, \tag{14a}$$

$$\mathbf{c}_i^H \triangleq -\mathbf{a}_i^H \sin\psi - \mathbf{a}_i^H e^{-\jmath\frac{\pi}{2}} \cos\psi. \tag{14b}$$

Then, exploiting the well-known *log-sum-exp* approximation, the objective (11a) is converted to

$$\max_i \{f_i, g_i\} \lessapprox \varepsilon \log \sum_{i=K(m-1)+1}^{mK} \left[\exp(f_i/\varepsilon) + \exp(g_i/\varepsilon)\right], \tag{15}$$

where $\varepsilon > 0$ is a relatively small number to maintain the approximation.

After obtaining the smooth and differentiable objective (15) for problem (11), the unit-modulus constraint (11b) of the IRS becomes the major challenge. Non-convex relaxation and alternating optimization based algorithms are very popular approaches for solving this problem. However, the relaxation-based algorithms may suffer significant performance loss and the alternating optimization algorithms may have slow convergence. To avoid these issues, we adopt the Riemannian-manifold-based algorithm, which directly solves this problem on the original feasible space instead of a relaxed convex version, and thus is able to provide a locally optimal solution with fast convergence [43]. Constraint (11b) forms an N-dimensional complex circle manifold

$$\mathcal{M}_{\text{cc}} \triangleq \left\{\boldsymbol{\theta}_m \in \mathbb{C}^N : \boldsymbol{\theta}_m^*(n)\boldsymbol{\theta}_m(n) = 1,\ \forall n\right\}, \tag{16}$$

which is a smooth Riemannian manifold equipped with an inner product defined on the tangent space:

$$T_{\boldsymbol{\theta}_m}\mathcal{M}_{\text{cc}} \triangleq \left\{\mathbf{p} \in \mathbb{C}^N : \Re\left\{\mathbf{p} \odot \boldsymbol{\theta}_m^*\right\} = \mathbf{0}_N,\ \forall n\right\}. \tag{17}$$

Then, problem (11) can be rewritten as

$$\min_{\boldsymbol{\theta}_m \in \mathcal{M}_{\text{cc}}} h\langle\boldsymbol{\theta}_m\rangle \triangleq \varepsilon \log \sum_{i=K(m-1)+1}^{mK} \left[\exp(f_i/\varepsilon) + \exp(g_i/\varepsilon)\right], \tag{18}$$

which is an unconstrained optimization problem on the Riemannian space $\mathcal{M}_{\text{cc}}$. Since each point on the manifold has a neighborhood homeomorphic to Euclidean space, the gradients of cost functions, distances, angles, etc., have counterparts on the Riemannian space, and efficient algorithms developed on the Euclidean space can be readily extended to the manifold space, e.g., the conjugate gradient (CG) algorithm. Therefore, in the following we use the CG algorithm on the Riemannian space, referred to as the Riemannian conjugate gradient (RCG) algorithm, to solve this problem.

To facilitate the RCG algorithm, we first derive the Euclidean gradient of $h\langle\boldsymbol{\theta}_m\rangle$ as

$$\nabla\, h\langle\boldsymbol{\theta}_m\rangle = \frac{\sum_{i=K(m-1)+1}^{mK} \left[\exp(f_i/\varepsilon)\mathbf{b}_i + \exp(g_i/\varepsilon)\mathbf{c}_i\right]}{\sum_{i=K(m-1)+1}^{mK} \left[\exp(f_i/\varepsilon) + \exp(g_i/\varepsilon)\right]}. \tag{19}$$

Algorithm 1: RCG algorithm to obtain $\boldsymbol{\theta}_m^\star$.

Input: $h\langle\boldsymbol{\theta}_m\rangle$.
Output: $\boldsymbol{\theta}_m^\star$.
1: Initialize $\boldsymbol{\theta}_{m,0} \in \mathcal{M}_{\text{cc}}$, $\mathbf{d}_0 = -\text{grad}_{\boldsymbol{\theta}_m} h\langle\boldsymbol{\theta}_{m,0}\rangle$.
2: **Repeat**
3: Choose Polak-Ribiere parameter η_p [43].
4: Calculate search direction $\mathbf{d}_p$ by (21).
5: Calculate step size ξ_p [43].
6: Obtain the update $\boldsymbol{\theta}_{m,p+1}$ by (22).
7: Calculate gradient $\text{grad}_{\boldsymbol{\theta}_m} h\langle\boldsymbol{\theta}_{m,p}\rangle$ by (20).
8: **Until convergence**

Then, the Riemannian gradient grad $h\langle\boldsymbol{\theta}_m\rangle$ can be obtained by projecting the Euclidean gradient $\nabla\, h\langle\boldsymbol{\theta}_m\rangle$ onto its corresponding Riemannian tangent space as follows:

$$\begin{aligned}\text{grad}\ h\langle\boldsymbol{\theta}_m\rangle &= \text{Proj}_{\boldsymbol{\theta}_m} \nabla h\langle\boldsymbol{\theta}_m\rangle \\ &= \nabla h\langle\boldsymbol{\theta}_m\rangle - \Re\left\{\nabla h\langle\boldsymbol{\theta}_m\rangle \odot \boldsymbol{\theta}_m^*\right\} \odot \boldsymbol{\theta}_m.\end{aligned} \tag{20}$$

Thus, in the p-th iteration of the RCG algorithm, the search direction $\mathbf{d}_p$ is

$$\mathbf{d}_p = -\text{grad}\ h\langle\boldsymbol{\theta}_{m,p-1}\rangle + \eta_p \mathbf{d}_{p-1}^{\text{t}}, \tag{21}$$

where $\boldsymbol{\theta}_{m,p-1}$ is the solution in the $(p-1)$-th iteration, and η_p is the Polak-Ribiere parameter [43]. Since the Riemannian gradient and search direction for the $(p-1)$-th iteration lie in different tangent spaces, an additional Riemannian transport operation is needed to map $\mathbf{d}_{p-1}$ into the tangent space of grad $h\langle\boldsymbol{\theta}_{m,p-1}\rangle$ denoted by $\mathbf{d}_{p-1}^{\text{t}}$. After choosing the step size ξ_p using the Armijo backtracking line search method [43], the p-th update is given by

$$\boldsymbol{\theta}_{m,p+1} = \text{Retr}_{\boldsymbol{\theta}_m}\left(\boldsymbol{\theta}_{m,p} + \xi_p \mathbf{d}_p\right), \tag{22}$$

where $\text{Retr}_{\boldsymbol{\theta}_m}(\cdot)$ indicates the retraction operation, mapping the point on the tangent space to the manifold.

Based on the above analysis, the locally optimal solution to each $\boldsymbol{\theta}_m^\star$ can be obtained using the RCG algorithm as summarized in Algorithm 1. Then, the minimum required power can be calculated by substituting $\boldsymbol{\theta}_m^\star, \forall m$ to (8). In addition, as proven in Theorem 4.3.1 of [43], Algorithm 1 is guaranteed to converge to a critical point where the Riemannian gradient equals zero.

C. Design for QoS Balancing

In this subsection, we consider the QoS balancing problem, which aims to maximize the minimum weighted QoS performance for a given transmit power. The optimization problem is formulated as

$$\max_{\boldsymbol{\theta}_m, \forall m} \min_{m,k} \ \rho_k \left[\Re\left\{\widetilde{r}_{m,k}\right\} \sin\psi - \left|\Im\left\{\widetilde{r}_{m,k}\right\}\right| \cos\psi\right] \tag{23a}$$

$$\text{s.t.}\ \widetilde{r}_{m,k} = \sqrt{P}\mathbf{h}_k^H \boldsymbol{\theta}_m e^{-\jmath\angle s_{m,k}},\ \forall m, k, \tag{23b}$$

$$|\boldsymbol{\theta}_m(n)| = 1,\ \forall m, n, \tag{23c}$$

where P is the maximum transmit power and $\rho_k > 0$ is the weight coefficient for the k-th user. It can be seen that this

problem is very similar to problem (10). Therefore, this QoS balancing problem can be solved with the algorithm proposed in Sec. II-B by setting $\alpha_k = \frac{1}{\rho_k \sqrt{P}}, \forall k$ in (10).

D. Design for Low-Resolution IRS

Since an IRS with infinite/high-resolution phase shifters would inevitably require higher hardware complexity and cost, low-resolution phase shifters are practically appealing. Thus, in this subsection, we investigate solutions for the case of low-resolution IRS.

With the continuous solution $\boldsymbol{\theta}_m^\star$ obtained as in Sec. II-B, a direct quantization operation as in [44] can be easily applied to seek the nearest discrete phase value by

$$\angle \boldsymbol{\theta}_m^B(n) = \left[\frac{\angle \boldsymbol{\theta}_m^\star(n)}{\Delta}\right]_{\mathrm{r}} \times \Delta, \tag{24}$$

where $\Delta \triangleq \frac{2\pi}{2^B}$ is the resolution of each reflecting elements controlled by B bits, and $[\cdot]_{\mathrm{r}}$ indicates the rounding operation. However, this method provides a suboptimal solution due to the quantization error, which may cause severe performance degradation for very low-resolution cases, e.g., 1-bit and 2-bit cases [8].

Thus, we investigate obtaining the optimal solutions by converting the optimization problem into a mixed-integer nonlinear program (MINLP) and solving it with an off-the-shelf algorithm. The low-resolution phase-shifts can be rewritten as

$$\boldsymbol{\theta}_m^B = \mathbf{Q}_m \mathbf{q}, \tag{25}$$

where the auxiliary vector $\mathbf{q} \triangleq [e^{\jmath\Delta}, e^{\jmath 2\Delta}, \ldots, e^{\jmath 2\pi}]^T$ contains all the possible phase values, $\mathbf{Q}_m \in \{0,1\}^{N\times 2^B}$ has only one non-zero element per row, and $\mathbf{Q}_m(n,j) = 1$ indicates the n-th element in $\boldsymbol{\theta}_m$ is $\mathbf{q}(j)$. Then, the optimization problem for the low-resolution IRS case is re-formulated as

$$\min_{\mathbf{Q}_m} \max_k \ \left|\Im\left\{\mathbf{a}_i^H \mathbf{Q}_m \mathbf{q}\right\}\right| \cos\psi - \Re\left\{\mathbf{a}_i^H \mathbf{Q}_m \mathbf{q}\right\} \sin\psi \tag{26a}$$

$$\text{s.t.} \quad \sum_{j=1}^{2^B} \mathbf{Q}_m(n,j) = 1, \ \forall n, \tag{26b}$$

$$\mathbf{Q}_m(n,j) \in \{0,1\}, \ \forall n, j, \tag{26c}$$

which is an MINLP problem and can be efficiently solved using the well-known branch-and-bound algorithm [45]. The details of this well-known algorithm are omitted for brevity. When the optimal $\mathbf{Q}_m^\star$ for problem (26) is found, the optimal low-resolution reflection coefficients $\boldsymbol{\theta}_m^{B\star}$ can be constructed as

$$\boldsymbol{\theta}_m^{B\star} = \mathbf{Q}_m^\star \mathbf{q}. \tag{27}$$

However, considering the required high computational complexity, the branch-and-bound algorithm is only suitable for the 1-bit or 2-bit cases.

In order to provide better performance than direct quantization and lower complexity than the branch-and-bound algorithm, we further propose an efficient heuristic algorithm to successively seek the conditionally optimal low-resolution solutions. Assuming that only the n-th element of $\boldsymbol{\theta}_m$ is unknown, the optimization problem is formulated as

$$\min_{\boldsymbol{\theta}_m(n)} \max_k \ \left|\Im\left\{c_i + a_{i,n}\boldsymbol{\theta}_m(n)\right\}\right| \cos\psi - \Re\left\{c_i + a_{i,n}\boldsymbol{\theta}_m(n)\right\} \sin\psi \tag{28a}$$

$$\text{s.t.} \quad \boldsymbol{\theta}_m(n) \in \left\{e^{\jmath\Delta}, e^{\jmath 2\Delta}, \ldots, e^{\jmath 2\pi}\right\}, \tag{28b}$$

where $c_i \triangleq \sum_{j=1, j\neq n}^{N} a_{i,j}\boldsymbol{\theta}_m(j)$, and $a_{i,j}$ denotes the j-th element of $\mathbf{a}_i^H$. Since in this case the number of feasible discrete values is not very large, an exhaustive search for the solution to (28) is affordable. With the obtained continuous $\boldsymbol{\theta}_m^\star$ as the initial value, we iteratively solve (28) for each element of the IRS until convergence is achieved.

E. Computational Complexity Analysis

The worst-case complexity of the RCG algorithm to obtain $\boldsymbol{\theta}_m^\star$ is of order $\mathcal{O}\{N^{1.5}\}$ [43]. Thus, the total complexity for the power minimization and QoS balancing problems with continuous IRS phase shifts is of order $\mathcal{O}\{\Omega^K N^{1.5}\}$. For low-resolution IRS, the complexity of the quantization operation in (24) is of order $\mathcal{O}\{2N\}$, which can be neglected compared with the complexity required to obtain the continuous solution. Thus, the total complexity for the low-resolution IRS scenario using quantization is also of order $\mathcal{O}\{\Omega^K N^{1.5}\}$. For B-bit IRS using the branch-and-bound algorithm, the optimization problem is a 2^B-dimensional integer program with N variables, whose complexity is of order $\mathcal{O}\{2^{3.5B}N^{2.5} + 2^{2.5B}N^{3.5}\}$ [45]. Thus, the total complexity for this scenario is of order $\mathcal{O}\{\Omega^K(2^{3.5B}N^{2.5} + 2^{2.5B}N^{3.5})\}$. The computational complexity of the branch-and-bound algorithm is exponential in B, and is obviously much higher than direct quantization. The complexity of the heuristic algorithm is of order $\mathcal{O}\{\Omega^K[N^{1.5} + K(2^B + N)]\}$, which is slightly higher than direct quantization but much lower than the branch-and-bound algorithm.

III. Joint Passive Reflection and Information Transmission System

A. System Model

In this section, we introduce the joint passive reflection and information transmission system as shown in Fig. 3, where the IRS is a dual-function device, i.e., it combines the passive reflection function as in the traditional IRS-assisted downlink MU-MISO systems [10] and the passive information transmission function as described in the previous section. In particular, the IRS with N passive reflecting elements enhances the primary information transmissions from an M-antenna BS to K single-antenna primary information receivers (PIRs) by adjusting its reflection coefficients. Meanwhile, it also transmits secondary information to one secondary information receiver (SIR) by selecting the proper reflection. The secondary information, e.g., environmental data, is collected from the surroundings by a sensor or IoT device. We assume that the K PIRs and one SIR[3] are separate receivers.

[3] We should emphasize that the results in this section can be easily generalized to the scenario with multiple SIRs.

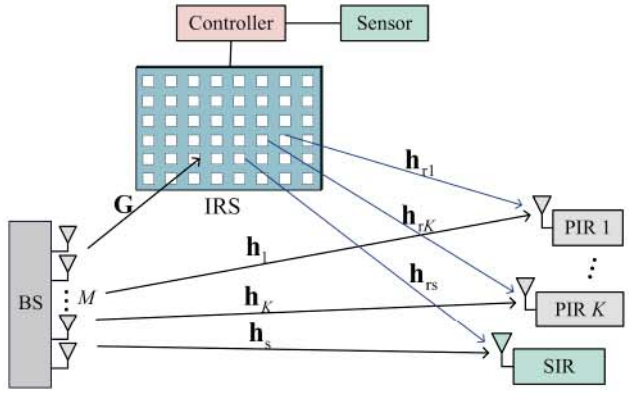

Fig. 3. Joint passive reflection and information transmission system, where IRS serves as a reflector and transmitter.

We emphasize that in the considered joint passive reflection and information transmission system, the primary function of the IRS is to enhance the active information transmissions from the BS to PIRs by passive reflection. The passive information transmission from the IRS to the SIR is the secondary task, which requires very low transmission rate. To perform the above dual functions, the IRS deployment and operation are quite different compared with the standalone passive information transmission system in the previous section. In the following, we present detailed system models for both primary and secondary information transmissions.

For the primary information transmissions, the active precoding at the BS and passive reflection at the IRS are jointly optimized. Specifically, non-linear symbol-level precoding is employed since it not only enhances the primary information transmissions by converting harmful MUI into useful signals, but also provides additional symbol-level DoFs for embedding secondary information. As before, assume that the primary information symbols for the K PIRs are independent Ω-PSK modulated symbols, and let $\mathbf{s}_m \triangleq [s_{m,1}, \ldots, s_{m,K}]^T, m = 1, \ldots, \Omega^K$ represent all possible symbol combinations for the K PIRs. The precoder for transmitting $\mathbf{s}_m$ is denoted by $\mathbf{x}_m \in \mathbb{C}^M$ and the signal received by the k-th PIR is

$$y_{m,k} = (\mathbf{h}_k^H + \mathbf{h}_{rk}^H \boldsymbol{\Theta} \mathbf{G})\mathbf{x}_m + n_k,\ m = 1, \ldots, \Omega^K, \quad (29)$$

where $\mathbf{h}_k \in \mathbb{C}^M$, $\mathbf{h}_{rk} \in \mathbb{C}^N$, and $\mathbf{G} \in \mathbb{C}^{N \times M}$ are the channels from the BS to the k-th PIR, from the IRS to the k-th PIR, and from the BS to IRS, respectively, $\boldsymbol{\Theta} \triangleq \mathrm{diag}\{\boldsymbol{\theta}\}$ is the reflection matrix, and $n_k \sim \mathcal{CN}(0, \sigma^2)$ is AWGN at the k-th PIR. Similar to Sec. II, the PIRs detect their desired symbols by simple hard decisions according to the pre-known constellation information. In addition, the QoS constraint for the PIRs is written as

$$\Re\{\widetilde{y}_{m,k}\} \sin\psi - |\Im\{\widetilde{y}_{m,k}\}| \cos\psi \geq \alpha_k,\ \forall m, k, \quad (30)$$

where $\widetilde{y}_{m,k} = (\mathbf{h}_k^H + \mathbf{h}_{rk}^H \boldsymbol{\Theta} \mathbf{G})\mathbf{x}_m e^{-\jmath \angle s_{m,k}}$ is the rotated noise-free signal as before.

For the secondary passive information transmission, we propose to embed the secondary information into the primary signals using the extra DoFs available in the reflection coefficients of the IRS. Since only a small amount of data is transmitted by the sensor in general, the rate of the secondary transmission is usually much lower than that of the primary transmissions. Therefore, we propose to embed "binary" secondary information symbols into the L primary signals by selecting the reflection matrix as either $\boldsymbol{\Theta}_0 \triangleq \mathrm{diag}\{\boldsymbol{\theta}_0\}$ or $\boldsymbol{\Theta}_1 \triangleq \mathrm{diag}\{\boldsymbol{\theta}_1\}$, depending on whether "0" or "1" is being sent by the sensor. In other words, the reflection matrix of the IRS is $\boldsymbol{\Theta}_0$ during L time slots when the transmitted binary secondary symbol is "0," and $\boldsymbol{\Theta}_1$ when it is "1". A smaller L will provide a higher secondary symbol rate, but usually also results in worse SER performance. Meanwhile, since the BS does not have access to the secondary information and the secondary information transmission should avoid affecting the primary information transmissions, both reflection matrices $\boldsymbol{\Theta}_0$ and $\boldsymbol{\Theta}_1$ should satisfy the QoS constraint for the PIRs in (30). The QoS constraint for the PIRs is thus re-written as

$$\Re\{\widetilde{y}_{m,k,0/1}\} \sin\psi - \left|\Im\{\widetilde{y}_{m,k,0/1}\}\right| \cos\psi \geq \alpha_k,\ \forall m, k, \quad (31)$$

where $\widetilde{y}_{m,k,0/1} = (\mathbf{h}_k^H + \mathbf{h}_{rk}^H \boldsymbol{\Theta}_{0/1} \mathbf{G})\mathbf{x}_m e^{-\jmath \angle s_{m,k}}$ and the subscript $0/1$ denotes whether the reflection matrix is either $\boldsymbol{\Theta}_0$ or $\boldsymbol{\Theta}_1$.

Before formulating the QoS constraint for the SIR, the detection strategy should be discussed since it is directly related to the QoS performance metric. To detect the secondary information at the SIR, the authors in [27], [28] proposed a two-step approach, which recovers the primary symbols first, and then utilizes the recovered primary symbols to decode the secondary symbols. On the other hand, the primary and secondary symbols in [30] were jointly recovered using a maximum-likelihood (ML) detector. However, requiring decoding of the much higher rate primary transmissions places an excessive computational burden on the SIR, which is only interested in the lower rate secondary information. Therefore, we propose a more efficient strategy to embed the secondary symbols, which facilitates a very simple hard decision detector.

In particular, the SIR detector simply extracts the binary embedded secondary information by evaluating the average received signal during the L time slots. To express the average of the SIR's signals collected during the L time slots, we first assume that, in the l-th time slot, $l = 1, \ldots, L$, the index of the primary transmitted symbol vector is $m_l \in \{1, \ldots, \Omega^K\}$. The signal received by the SIR is thus expressed as

$$y_{m_l,\mathrm{s},0/1} = (\mathbf{h}_\mathrm{s}^H + \mathbf{h}_\mathrm{rs}^H \boldsymbol{\Theta}_{0/1} \mathbf{G})\mathbf{x}_{m_l} + n_\mathrm{s}, \quad (32)$$

where the subscript "s" denotes the SIR, $\mathbf{h}_\mathrm{s}$ and $\mathbf{h}_\mathrm{rs}$ are respectively the channel vectors from the BS to SIR and from the IRS to SIR,[4] and $n_\mathrm{s} \sim \mathcal{CN}(0, \sigma^2)$ is AWGN at the SIR. Denoting the set of transmitted symbol indices during the L time slots as $\mathcal{I} \triangleq \{m_1, \ldots, m_L\}$, the average received signal at the SIR is

[4]Although CSI acquisition in IRS-assisted systems is still a challenging task, accurate CSI can be obtained with existing channel estimation algorithms [8] [38]-[42]. In order to focus on characterizing the performance upper bound of the joint passive reflection and information transmission system, we assume perfect CSI in this paper. In addition, the CSI of the primary information receivers and secondary information receiver can be distinguished at the BS by different pilot sequences or using time division duplexing (TDD).

expressed as

$$\begin{aligned}\overline{r}_{0/1} &= \frac{1}{L}\sum_{m_l\in\mathcal{I}} y_{m_l,\mathrm{s},0/1} \\ &= \begin{cases} \frac{1}{L}(\mathrm{h}_\mathrm{s}^H + \mathrm{h}_\mathrm{rs}^H\boldsymbol{\Theta}_0\mathrm{G})\sum_{m_l\in\mathcal{I}}\mathrm{x}_{m_l} + n_\mathrm{s} : H_0, \\ \frac{1}{L}(\mathrm{h}_\mathrm{s}^H + \mathrm{h}_\mathrm{rs}^H\boldsymbol{\Theta}_1\mathrm{G})\sum_{m_l\in\mathcal{I}}\mathrm{x}_{m_l} + n_\mathrm{s} : H_1. \end{cases}\end{aligned} \tag{33}$$

With the principle of binary-PSK (BPSK) modulation, the secondary information is detected as "1" if $\Re\{\overline{r}\} > 0$, or "0" if $\Re\{\overline{r}\} < 0$. Inspired by symbol-level precoding, we utilize the CI region concept for the secondary information transmission design. The CI regions for the SIR are defined as follows

$$\Re\left\{\frac{1}{L}(\mathrm{h}_\mathrm{s}^H + \mathrm{h}_\mathrm{rs}^H\boldsymbol{\Theta}_0\mathrm{G})\sum_{m_l\in\mathcal{I}}\mathrm{x}_{m_l}\right\} \le -\beta : H_0, \tag{34a}$$

$$\Re\left\{\frac{1}{L}(\mathrm{h}_\mathrm{s}^H + \mathrm{h}_\mathrm{rs}^H\boldsymbol{\Theta}_1\mathrm{G})\sum_{m_l\in\mathcal{I}}\mathrm{x}_{m_l}\right\} \ge \beta : H_1, \tag{34b}$$

where $\beta > 0$ is the QoS requirement that denotes the minimum Euclidean distance between the average received noise-free signal and its decision boundary. During the L time slots, $\sum_{m_l\in\mathcal{I}}\mathrm{x}_{m_l}$ can take on $C_{\Omega^K}^L$ possible values, which cannot be practically accounted for in the precoding and reflection design. Thus, we propose to simplify this constraint by decomposing the summation into individual terms. Then, the QoS constraint for the SIR is re-formulated as

$$\Re\left\{(\mathrm{h}_\mathrm{s}^H + \mathrm{h}_\mathrm{rs}^H\boldsymbol{\Theta}_0\mathrm{G})\mathrm{x}_m\right\} \le -\beta,\ \forall m, \tag{35a}$$

$$\Re\left\{(\mathrm{h}_\mathrm{s}^H + \mathrm{h}_\mathrm{rs}^H\boldsymbol{\Theta}_1\mathrm{G})\mathrm{x}_m\right\} \ge \beta,\ \forall m, \tag{35b}$$

which is a stricter constraint than (34) since the SIR's received noise-free signal is forced to satisfy the QoS requirement in each time slot, rather than the average signal over all L time slots.

Based on the above, the procedure for the IRS-based simultaneous primary and secondary information transmissions is straightforward. With given QoS requirements for the PIRs and SIR, the symbol-level precoders $\mathrm{x}_m, \forall m$, and reflection vectors $\boldsymbol{\theta}_0$, $\boldsymbol{\theta}_1$ are jointly optimized at the BS. Then, the optimized reflection vectors $\boldsymbol{\theta}_0$, $\boldsymbol{\theta}_1$ are transmitted to the IRS controller through a dedicated control link. During the transmission phase, the BS sends the precoded signal x_m in each time slot according to the corresponding primary information symbol vector s_m. Meanwhile, the controller adjusts the IRS reflection vector $\boldsymbol{\theta}_0$ or $\boldsymbol{\theta}_1$ every L time slots according to the binary secondary information.

The design of the precoding vectors $\mathrm{x}_m, \forall m$, and the reflection vectors $\boldsymbol{\theta}_0$ and $\boldsymbol{\theta}_1$ leads to a joint passive reflection and information transmission problem that is more complicated than that in the previous section. In the following subsections, we propose efficient algorithms to solve the resulting joint power minimization and QoS balancing optimization problems.

B. Design for Power Minimization

In this subsection, we investigate the joint design of the precoding and reflection vectors to minimize the transmit power while guaranteeing the QoS for the PIRs (31) and SIR (35). Accordingly, the general problem can be formulated as

$$\min_{\substack{\mathrm{x}_m,\forall m,\\ \boldsymbol{\theta}_0,\boldsymbol{\theta}_1}} \sum_{m=1}^{\Omega^K}\|\mathrm{x}_m\|^2 \tag{36a}$$

$$\text{s.t.}\quad \Re\left\{\widetilde{y}_{m,k,0/1}\right\}\sin\psi - \left|\Im\left\{\widetilde{y}_{m,k,0/1}\right\}\right|\cos\psi \ge \alpha_k,$$

$$\widetilde{y}_{m,k,0/1} = (\mathrm{h}_k^H + \mathrm{h}_{\mathrm{r}k}^H\boldsymbol{\Theta}_{0/1}\mathrm{G})\mathrm{x}_m e^{-\jmath\angle s_{m,k}},\ \forall m,k, \tag{36b}$$

$$\Re\left\{(\mathrm{h}_\mathrm{s}^H + \mathrm{h}_\mathrm{rs}^H\boldsymbol{\Theta}_0\mathrm{G})\mathrm{x}_m\right\} \le -\beta,\ \forall m, \tag{36c}$$

$$\Re\left\{(\mathrm{h}_\mathrm{s}^H + \mathrm{h}_\mathrm{rs}^H\boldsymbol{\Theta}_1\mathrm{G})\mathrm{x}_m\right\} \ge \beta,\ \forall m, \tag{36d}$$

$$\boldsymbol{\Theta}_{0/1} = \mathrm{diag}\{\boldsymbol{\theta}_{0/1}\},\quad |\boldsymbol{\theta}_{0/1}(n)| = 1,\ \forall n. \tag{36e}$$

Note that this is a non-convex optimization problem that is difficult to solve due to the following reasons. First, the precoders $\mathrm{x}_m, \forall m$ and the reflection vectors $\boldsymbol{\theta}_0$, $\boldsymbol{\theta}_1$ are intricately coupled in the QoS constraints (36b)-(36d). Second, the unit-modulus constraint of the reflection vectors in constraint (36e) is non-convex. To address this problem, we propose to partition all optimization variables into two blocks (i.e., $\mathrm{x}_m, \forall m$ and $\boldsymbol{\theta}_0$, $\boldsymbol{\theta}_1$), and then solve each of the sub-problem alternately until convergence is achieved.

With fixed $\boldsymbol{\theta}_0$ and $\boldsymbol{\theta}_1$, the compound channel from the BS to the k-th PIR and SIR can be concisely expressed as

$$\begin{aligned}\widetilde{\mathrm{h}}_{k,0/1}^H &\triangleq \mathrm{h}_k^H + \mathrm{h}_{\mathrm{r}k}^H\boldsymbol{\Theta}_{0/1}\mathrm{G},\ \forall k, \\ \widetilde{\mathrm{h}}_{\mathrm{s},0/1}^H &\triangleq \mathrm{h}_\mathrm{s}^H + \mathrm{h}_\mathrm{rs}^H\boldsymbol{\Theta}_{0/1}\mathrm{G}.\end{aligned} \tag{37}$$

Similarly, the precoder vectors $\mathrm{x}_m, m = 1,\ldots,\Omega^K$, are independent of each other for the power minimization problem, and thus it can be divided into Ω^K sub-problems to be solved in parallel. In particular, the m-th sub-problem for optimizing x_m is given by

$$\min_{\mathrm{x}_m}\ \|\mathrm{x}_m\|^2 \tag{38a}$$

$$\begin{aligned}\text{s.t.}\quad &\Re\{\widetilde{\mathrm{h}}_{k,0/1}^H\mathrm{x}_m e^{-\jmath\angle s_{m,k}}\}\sin\psi \\ &\quad - |\Im\{\widetilde{\mathrm{h}}_{k,0/1}^H\mathrm{x}_m e^{-\jmath\angle s_{m,k}}\}|\cos\psi \ge \alpha_k,\ \forall k,\end{aligned} \tag{38b}$$

$$\Re\{\widetilde{\mathrm{h}}_{\mathrm{s},0}^H\mathrm{x}_m\} \le -\beta, \tag{38c}$$

$$\Re\{\widetilde{\mathrm{h}}_{\mathrm{s},1}^H\mathrm{x}_m\} \ge \beta, \tag{38d}$$

which is convex and can be solved by standard optimization tools, e.g., CVX. In addition, the more efficient gradient projection algorithm [33] can be employed to solve (38), although the details are omitted for brevity.

After obtaining precoder vectors $\mathrm{x}_m, m = 1,\ldots,\Omega^K$, the reflection design problem is reduced to a feasibility-check problem without an objective, which may generate many solutions and lead to different convergence rates. Thus, we utilize an auxiliary variable t to impose stricter QoS constraints, which can provide more freedom for power minimization in the next iteration and accelerate the convergence. To this end, the IRS reflection design problem is transformed to

Algorithm 2: Joint Symbol-Level Precoding and Reflection Design for the Power Minimization Problem.

Input: $\mathbf{h}_k, \mathbf{h}_{rk}, \alpha_k, \forall k, \mathbf{G}, \mathbf{h}_s, \mathbf{h}_{rs}, \Omega, \sigma^2, \beta$.
Output: $\mathbf{X}^\star, \boldsymbol{\theta}_0^\star, \boldsymbol{\theta}_1^\star$.
1: Initialize $\boldsymbol{\theta} \in \mathcal{M}_{cc}$.
2: **Repeat**
3: Calculate each precoder vector $\mathbf{x}_m^\star, \forall m$ by solving (38).
4: Obtain continuous $\boldsymbol{\theta}^\star$ by solving (43).
5: Construct reflection vectors $\boldsymbol{\theta}_0^\star$ and $\boldsymbol{\theta}_1^\star$ by (44).
6: Calculate low-resolution solutions using (24).
7: **Until convergence**

$$\max_{t,\boldsymbol{\theta}_0,\boldsymbol{\theta}_1} \quad t \tag{39a}$$

$$\text{s.t.} \quad \Re\left\{\widetilde{y}_{m,k,0/1}\right\}\sin\psi - \left|\Im\left\{\widetilde{y}_{m,k,0/1}\right\}\right|\cos\psi \geq \alpha_k t,$$
$$\widetilde{y}_{m,k,0/1} = (\mathbf{h}_k^H + \mathbf{h}_{rk}^H\boldsymbol{\Theta}_0\mathbf{G})\mathbf{x}_m e^{-\jmath\angle s_{m,k}}, \ \forall m,k, \tag{39b}$$

$$-\Re\left\{(\mathbf{h}_s^H + \mathbf{h}_{rs}^H\boldsymbol{\Theta}_0\mathbf{G})\mathbf{x}_m\right\} \geq \beta t, \ \forall m, \tag{39c}$$

$$\Re\left\{(\mathbf{h}_s^H + \mathbf{h}_{rs}^H\boldsymbol{\Theta}_1\mathbf{G})\mathbf{x}_m\right\} \geq \beta t, \ \forall m, \tag{39d}$$

$$\boldsymbol{\Theta}_{0/1} = \text{diag}\{\boldsymbol{\theta}_{0/1}\}, \quad |\boldsymbol{\theta}_{0/1}(n)| = 1, \ \forall n, \tag{39e}$$

where $t \geq 1$ since the reflection coefficients obtained from the previous iteration satisfy the QoS requirements. Thus, after solving (39), a better QoS than the original requirement is achieved for the obtained precoders in the current iteration. In order to solve this multivariate problem, we convert it into a univariate problem by eliminating t, combing $\boldsymbol{\theta}_0$ and $\boldsymbol{\theta}_1$ into a single vector, and exploiting the RCG algorithm to handle the unit-modulus constraint, as detailed below.

First, in order to re-arrange the optimization problem in (39) to a univariate problem, we define

$$\boldsymbol{\theta} \triangleq [\boldsymbol{\theta}_0^T, \boldsymbol{\theta}_1^T]^T,$$
$$a_{m,k} \triangleq \mathbf{h}_k^H\mathbf{x}_m e^{-\jmath\angle s_{m,k}}, \ \forall m,k,$$
$$a_{m,K+1} \triangleq \mathbf{h}_s^H\mathbf{x}_m, \ \forall m,$$
$$\mathbf{b}_{m,k,0/1}^H \triangleq \mathbf{e}_{0/1}^T \otimes \left\{\mathbf{h}_{rk}^H\text{diag}\{\mathbf{G}\mathbf{x}_m e^{-\jmath\angle s_{m,k}}\}\right\}, \ \forall m,k,$$
$$\mathbf{b}_{m,K+1,0/1}^H \triangleq \mathbf{e}_{0/1}^T \otimes \left\{\mathbf{h}_{rs}^H\text{diag}\{\mathbf{G}\mathbf{x}_m\}\right\}, \ \forall m,$$

where $\mathbf{e}_0 \triangleq [1,0]^T, \mathbf{e}_1 \triangleq [0,1]^T$. Thus, we have the following concise representations of the received signals

$$\widetilde{y}_{m,k,0/1} = a_{m,k} + \mathbf{b}_{m,k,0/1}^H\boldsymbol{\theta}, \ \forall m,k,$$
$$(\mathbf{h}_s^H + \mathbf{h}_{rs}^H\boldsymbol{\Theta}_{0/1}\mathbf{G})\mathbf{x}_m = a_{m,K+1} + \mathbf{b}_{m,K+1,0/1}^H\boldsymbol{\theta}, \ \forall m. \tag{40}$$

Then, the optimization problem (39) is converted to

$$\max_{\boldsymbol{\theta},t} \quad t \tag{41a}$$

$$\text{s.t.} \quad f_i \triangleq \Re\{\mathbf{b}_i^H\boldsymbol{\theta}\} + w_i \leq -t, \ \forall i, \tag{41b}$$

$$g_i \triangleq \Re\{\mathbf{c}_i^H\boldsymbol{\theta}\} + z_i \leq -t, \ \forall i, \tag{41c}$$

$$|\boldsymbol{\theta}(n)| = 1, \ n = 1,\ldots,2N, \tag{41d}$$

where the expressions for $\mathbf{b}_i$ and $\mathbf{c}_i$ are similar to (14) and omitted for brevity. The constant terms w_i and z_i, $i = 1,\ldots,2(K+1)\Omega^K$, are expressed as

$$\begin{aligned} w_{2j-1} &= w_{2j} = -a_{m,k}\left(\sin\psi - e^{-\jmath\frac{\pi}{2}}\cos\psi\right)/\alpha_k, \\ w_{2K\Omega^K+m} &= a_{m,K+1}/\beta, \\ z_{2j-1} &= z_{2j} = -a_{m,k}\left(\sin\psi + e^{-\jmath\frac{\pi}{2}}\cos\psi\right)/\alpha_k, \\ z_{2K\Omega^K+m} &= -a_{m,K+1}/\beta, \end{aligned} \tag{42}$$

where $j = K(m-1)+k$. According to (41b) and (41c), we have $-t \geq \max\{f_i, g_i, \forall i\}$, thus problem (41) is further transformed to the following univariate problem

$$\min_{\boldsymbol{\theta}} \ \max_i \ \{f_i, g_i\} \tag{43a}$$

$$\text{s.t.} \quad |\boldsymbol{\theta}(n)| = 1, \ n = 1,\ldots,2N, \tag{43b}$$

which exhibits a similar form as problem (11). Therefore, we exploit the log-sum-exp approximation to handle the non-differentiable max value function, and then utilize the RCG algorithm to tackle the non-convex unit-modulus constraint. The solution to problem (43) follows the same procedures as in Sec. II-B, and thus the details are omitted here.

After obtaining $\boldsymbol{\theta}^\star$, the reflection vectors $\boldsymbol{\theta}_0^\star$ and $\boldsymbol{\theta}_1^\star$ can be extracted by

$$\boldsymbol{\theta}_0^\star = \boldsymbol{\theta}^\star(1:N), \quad \boldsymbol{\theta}_1^\star = \boldsymbol{\theta}^\star(N+1:2N). \tag{44}$$

For the low-resolution cases, we adopt the most efficient direct quantization method as in (24).

In summary, given random initial reflection vectors, the precoder vectors $\mathbf{x}_m, \forall m$, and reflection vectors $\boldsymbol{\theta}_0, \boldsymbol{\theta}_1$, are iteratively updated by solving problems (38) and (43) until convergence is achieved. The details of this joint symbol-level precoding and reflection design algorithm for the power minimization problem are summarized in Algorithm 2. Since the reflection design is suboptimal, monotonic convergence cannot be theoretically guaranteed. Alternatively, we provide numerical results in Sec. IV to show the convergence.

C. Design for QoS Balancing

In this subsection, we solve the QoS balancing problem for both PIRs and the SIR, which maximizes the minimum weighted QoS for a given average transmit power budget P and is formulated as

$$\max_{\substack{\mathbf{x}_m,\forall m,\\ \boldsymbol{\theta}_0,\boldsymbol{\theta}_1}} \quad t \tag{45a}$$

$$\text{s.t.} \quad t \leq \rho_k\left[\Re\{\widetilde{y}_{m,k,0/1}\}\sin\psi - |\Im\{\widetilde{y}_{m,k,0/1}\}|\cos\psi\right],$$
$$\widetilde{y}_{m,k,0/1} = (\mathbf{h}_k^H + \mathbf{h}_{rk}^H\boldsymbol{\Theta}_{0/1}\mathbf{G})\mathbf{x}_m e^{-\jmath\angle s_{m,k}}, \ \forall m,k, \tag{45b}$$

$$t \leq -\varrho\Re\{(\mathbf{h}_s^H + \mathbf{h}_{rs}^H\boldsymbol{\Theta}_0\mathbf{G})\mathbf{x}_m\}, \ \forall m, \tag{45c}$$

$$t \leq \varrho\Re\{(\mathbf{h}_s^H + \mathbf{h}_{rs}^H\boldsymbol{\Theta}_1\mathbf{G})\mathbf{x}_m\}, \ \forall m, \tag{45d}$$

$$\boldsymbol{\Theta}_{0/1} = \text{diag}\{\boldsymbol{\theta}_{0/1}\}, \quad |\boldsymbol{\theta}_{0/1}(n)| = 1, \ \forall n, \tag{45e}$$

$$\sum_{m=1}^{\Omega^K} \|\mathbf{x}_m\|^2 \leq P\Omega^K, \tag{45f}$$

where ρ_k and ϱ are the QoS weights for the k-th PIR and SIR, respectively. As before, we decompose this large-scale optimization problem into several sub-problems and iteratively solve them.

With given reflection vectors $\boldsymbol{\theta}_0$ and $\boldsymbol{\theta}_1$, the compound channels $\widetilde{\mathbf{h}}_{k,0/1}^H$ and $\widetilde{\mathbf{h}}_{\mathrm{s},0/1}^H$ can be obtained by (37), and the precoding design problem is rewritten as

$$\max_{\mathbf{x}_m,\forall m,t} \quad t \tag{46a}$$

$$\text{s.t.} \quad t \leq \rho_k \Big[\Re\{\widetilde{\mathbf{h}}_{k,0/1}^H \mathbf{x}_m e^{-\jmath\angle s_{m,k}}\} \sin\psi - |\Im\{\widetilde{\mathbf{h}}_{k,0/1}^H \mathbf{x}_m e^{-\jmath\angle s_{m,k}}\}| \cos\psi\Big], \ \forall m, k, \tag{46b}$$

$$t \leq -\varrho\Re\{\widetilde{\mathbf{h}}_{\mathrm{s},0}^H \mathbf{x}_m\}, \ \forall m, \tag{46c}$$

$$t \leq \varrho\Re\{\widetilde{\mathbf{h}}_{\mathrm{s},1}^H \mathbf{x}_m\}, \ \forall m, \tag{46d}$$

$$\sum_{m=1}^{\Omega^K} \|\mathbf{x}_m\|^2 \leq P\Omega^K, \tag{46e}$$

which is a convex optimization problem. In order to reduce the computational complexity, we still attempt to decompose it into Ω^K sub-problems and deal with the small-scale $\mathbf{x}_m$ individually. However, the average power constraint (46e) couples the design of each precoder since the total power must be balanced between them. Thus, we first explore the relationship between the objective value and the power constraint for each precoder, and then solve the power allocation problem. In the end, the optimal precoders are obtained based on the obtained allocated power.

Assuming that the transmit power allocated to $\mathbf{x}_m$ is $p_m, p_m > 0$ and $\sum_{m=1}^{\Omega^K} p_m = P\Omega^K$, the m-th sub-problem of (46) can be formulated as

$$\max_{\mathbf{x}_m,t_m} \quad t_m \tag{47a}$$

$$\text{s.t.} \quad t_m \leq \rho_k \Big[\Re\{\widetilde{\mathbf{h}}_{k,0/1}^H \mathbf{x}_m e^{-\jmath\angle s_{m,k}}\} \sin\psi - |\Im\{\widetilde{\mathbf{h}}_{k,0/1}^H \mathbf{x}_m e^{-\jmath\angle s_{m,k}}\}| \cos\psi\Big], \ \forall k, \tag{47b}$$

$$t_m \leq -\varrho\Re\{\widetilde{\mathbf{h}}_{\mathrm{s},0}^H \mathbf{x}_m\}, \tag{47c}$$

$$t_m \leq \varrho\Re\{\widetilde{\mathbf{h}}_{\mathrm{s},1}^H \mathbf{x}_m\}, \tag{47d}$$

$$\|\mathbf{x}_m\|^2 \leq p_m, \tag{47e}$$

where t_m is the minimum weighted QoS for precoder $\mathbf{x}_m$. We assume that the optimal solution for this problem is $\mathbf{x}_m^\star$ and $t_m^\star$. Notice that the norm of $\mathbf{x}_m^\star$ is proportional to $t_m^\star$ and $\sqrt{p_m}$, and thus the QoS balancing and power minimization problems will yield the same optimal solutions within a scaling that depends on the allocated power. Thus, we can obtain a scaled version of $\mathbf{x}_m^\star$ by solving the power minimization problem (38) with constraints $\alpha_k = \frac{t_0}{\rho_k}, \forall k$, $\beta = \frac{t_0}{\varrho}$, where $t_0 > 0$ is an arbitrary QoS requirement. After obtaining the optimal solution $\widetilde{\mathbf{x}}_m^\star$ of (38), the optimal solution $\mathbf{x}_m^\star$ and $t_m^\star$ of problem (47) can be obtained by scaling as

$$\mathbf{x}_m^\star = \frac{\sqrt{p_m}\widetilde{\mathbf{x}}_m^\star}{\|\widetilde{\mathbf{x}}_m^\star\|}, \quad t_m^\star = \frac{\sqrt{p_m}t_0}{\|\widetilde{\mathbf{x}}_m^\star\|}. \tag{48}$$

Then, we need to find the optimal power allocation p_m to balance the QoS requirement $t_m^\star$, which is formulated as

$$\max_{p_m,\forall m,t} \quad t \tag{49a}$$

$$\text{s.t.} \quad t \leq t_m^\star = \frac{\sqrt{p_m}t_0}{\|\widetilde{\mathbf{x}}_m^\star\|}, \ \forall m, \tag{49b}$$

$$\sum_{m=1}^{\Omega^K} p_m \leq P\Omega^K. \tag{49c}$$

Similarly, the optimal solution of this problem can also be obtained by solving the corresponding power minimization problem:

$$\min_{p_m,\forall m} \quad \sum_{m=1}^{\Omega^K} p_m \tag{50a}$$

$$\text{s.t.} \quad \sqrt{p_m} \geq \frac{\|\widetilde{\mathbf{x}}_m^\star\|}{t_0}, \forall m, \tag{50b}$$

which has the same form as problem (38) and can be efficiently solved using the projected gradient-based algorithm. Then, substituting the obtained power allocation p_m into (48), the precoder for the original QoS balancing problem (45) can be calculated.

In summary, the precoding design problem (46) is solved in three steps: *i)* Solving the power minimization problem (38) with an arbitrary QoS requirement t_0 and obtaining its optimal solution $\widetilde{\mathbf{x}}_m^\star$; *ii)* obtaining the power allocation $p_m, \forall m$, by solving problem (50); *iii)* calculating the solution $\mathbf{x}_m^\star$ by substituting p_m into (48).

With fixed precoding vectors $\mathbf{x}_m, \forall m$, the design of the reflection coefficients is similar to problem (39), and can be solved using the algorithm proposed in the previous subsection by setting $\alpha_k = \frac{1}{\rho_k}, \forall k$, and $\beta = \frac{1}{\varrho}$.

With the previous developments, the joint symbol-level precoding and reflection design for the QoS balancing problem (45) is straightforward and is summarized in Algorithm 3. Given random initial reflection vectors, problem (46) and (39) are iteratively solved to obtain the precoding vectors $\mathbf{x}_m, \forall m$, and the reflection vectors $\boldsymbol{\theta}_0$ and $\boldsymbol{\theta}_1$ until convergence is met.

D. Computational Complexity Analysis

For the power minimization problem, the computational complexity using the projected gradient algorithm to solve for $\mathbf{x}_m$ is of order $\mathcal{O}\{M^3\}$. The complexity required to obtain the reflection vectors is of order $\mathcal{O}\{(2\,N)^{1.5}\}$. Thus, the total computational complexity to solve the power minimization problem is of order $\mathcal{O}\{\Omega^K[M^3 + (2\,N)^{1.5}]\}$. For the QoS balancing problem, the computational complexity of the three steps required to obtain the precoders is of order $\mathcal{O}\{\Omega^K M^3\}$,

Algorithm 3: Joint Symbol-Level Precoding and Reflection Design for the QoS Balancing Problem.

Input: h_k, $\mathrm{h}_{\mathrm{r}k}$, ρ_k, $\forall k$, G, h_{s}, h_{rs}, Ω, σ^2, ϱ, t_0.
Output: $\mathrm{X}^\star$, $\theta_0^\star$, $\theta_1^\star$.
1: Initialize $\theta \in \mathcal{M}_{\mathrm{cc}}$.
2: **Repeat**
3: Calculate each precoder vector $\widetilde{\mathrm{x}}_m^\star, \forall m$ by solving (38).
4: Obtain power allocation $p_m, \forall m$ by solving (50).
5: Calculate $\mathrm{x}_m^\star$ by (48).
6: Obtain continuous $\theta^\star$ by solving (43).
7: Construct reflection vectors $\theta_0^\star$ and $\theta_1^\star$ by (44).
8: Calculate low-resolution solutions using (24).
9: **Until convergence**

$\mathcal{O}\{\Omega^{3K}\}$, and $\mathcal{O}\{M\Omega^K\}$, respectively. Thus, the total computational complexity of the QoS balancing algorithm is of order $\mathcal{O}\{\Omega^K(M^3+\Omega^{2K})+(2N)^{1.5}\}$.

IV. Simulation Results

In this section, we provide simulation results to demonstrate the feasibility of IRS-based passive information transmission and illustrate the effectiveness of our proposed algorithms. We adopt the popular settings in this field as in [10]. The noise power at all receivers is $\sigma^2 = -80$dBm. The constellation order is $\Omega = 4$, corresponding to QPSK. The path-loss is modelled as $\mathrm{PL}(d) = C_0(d_0/d)^\iota$, where $C_0 = -30$dB, $d_0 = 1$m, d is the link distance, and ι is the path-loss exponent. The small-scale Rician fading channel model is adopted for all links. For example, the channel from the BS to the IRS G is modelled as

$$\mathrm{G} = \sqrt{\frac{\kappa}{\kappa+1}}\mathrm{G}^{\mathrm{LoS}} + \sqrt{\frac{1}{\kappa+1}}\mathrm{G}^{\mathrm{NLoS}}, \tag{51}$$

where κ is the Rician factor set as 3 dB, $\mathrm{G}^{\mathrm{LoS}}$ is the line-of-sight (LoS) component determined by the geometric locations of the BS and the IRS, and $\mathrm{G}^{\mathrm{NLoS}}$ is the non-LoS (NLoS) Rayleigh fading component.

A. Passive Information Transmission System

In this subsection, we present simulation results for the passive information transmission system in Sec. II. We assume that $K = 3$ users are randomly distributed 100 m away from the IRS, and the path-loss exponent is set as $\kappa = 3$. For simplicity, we assume that the QoS requirements and weights for all users are the same, i.e., $\alpha_k = \alpha$, $\rho_k = \rho = 1$, $\forall k$.

Fig. 4 shows the average transmit power versus the QoS requirement α for the power minimization problem, including both the continuous and low-resolution cases. The 2, 3, 4, and 5-bit resolution cases using the direct quantization and heuristic algorithms in Sec. II-D are referred to as "Quantize, 2-bit"-"Quantize, 5-bit," and "Heuristic, 2-bit"-"Heuristic, 5-bit," respectively. The cases with 1-bit resolution are not shown due to their severely degraded performance. Since the

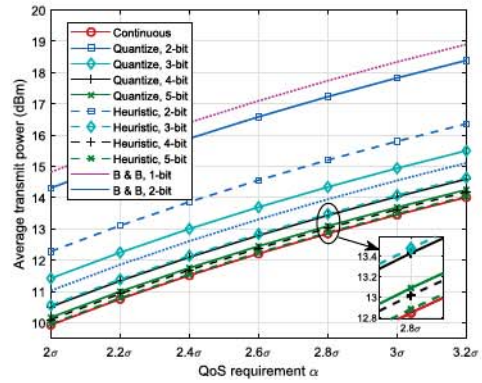

Fig. 4. Average transmit power versus QoS requirement α ($K = 3$, $N = 100$).

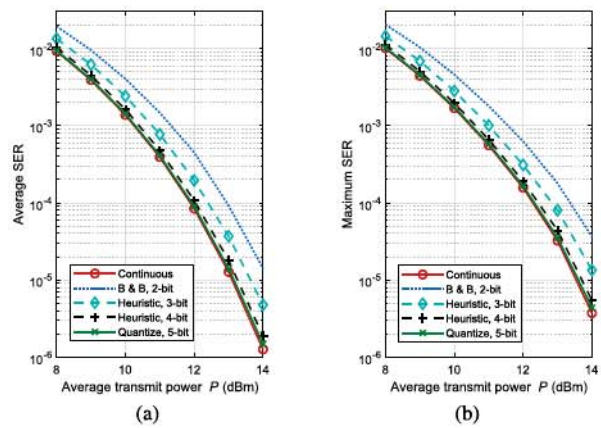

Fig. 5. SER versus average transmit power P ($K = 3$, $N = 100$). (a) Average SER versus P. (b) Maximum SER versus P.

optimal branch-and-bound algorithm has unaffordable exponential complexity for high-resolution cases, only the 1-bit and 2-bit cases are included, which are denoted as "B & B, 1-bit" and "B & B, 2-bit," respectively. It can be seen that the continuous scheme achieves the best performance given its flexibility in specifying the phase-shifts. Whereas for a given finite resolution, the branch-and-bound algorithm provides the best performance and the direct quantization method has the worst performance, as expected given their different levels of computational complexity. The choice of the algorithm and the resolution of the phase quantization requires a tradeoff between performance and complexity. For 5-bit or higher resolution, the computational complexity is a more dominant factor in practice, since the performance is already sufficiently close to that with infinite resolution at the IRS. For the 3-bit and 4-bit cases, the heuristic algorithm is a good choice in the sense that it provides better performance than direct quantization with affordable computational complexity. For the very low-resolution 1-bit and 2-bit cases, the optimal branch-and-bound algorithm provides much better performance. However, even using the optimal branch-and-bound algorithm, the 1-bit case still suffers a severe performance loss, requiring almost 5 dBm extra power to achieve the same performance as with continuous phase control. Thus, in Fig. 5 we choose the branch-and-bound algorithm for

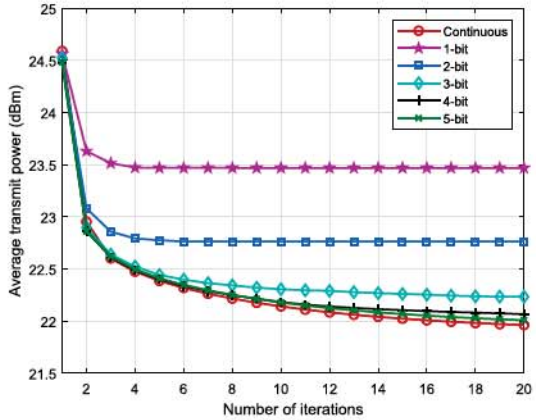

Fig. 6. Average transmit power versus the number of iterations ($K = 3, N = 100, \alpha = 2.5\sigma, \beta = 0.5\sigma$).

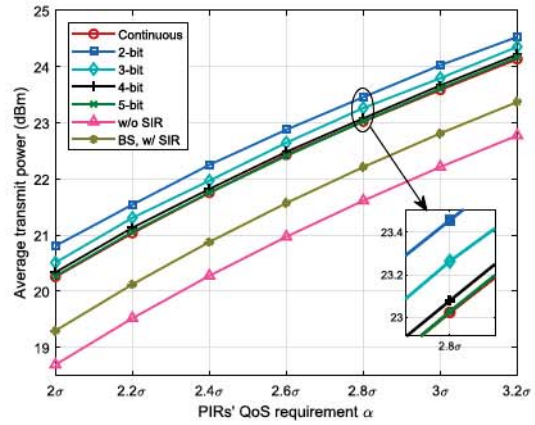

Fig. 7. Average transmit power versus PIRs' QoS requirement α ($K = 3$, $N = 100$, $\beta = 0.5\sigma$).

the 2-bit case, the heuristic algorithm for the 3-bit and 4-bit cases, and the direct quantization method for the 5-bit case to strike a balance between computational complexity and performance.

For the QoS balancing problem, we plot the SER versus the average transmit power P in Fig. 5. Since the weight coefficients ρ_k for all receivers are the same, the average and maximum SER of all receivers are plotted in Figs. 5(a) and 5(b), respectively, to show the QoS balancing performance. The difference between the average and maximum SER is very small, which verifies the QoS balancing between all receivers. In addition, it is encouraging to see that the 4-bit and 5-bit schemes achieve almost the same performance as the continuous scheme, and the performance loss of the 2-bit and 3-bit schemes is only 0.5-1 dBm.

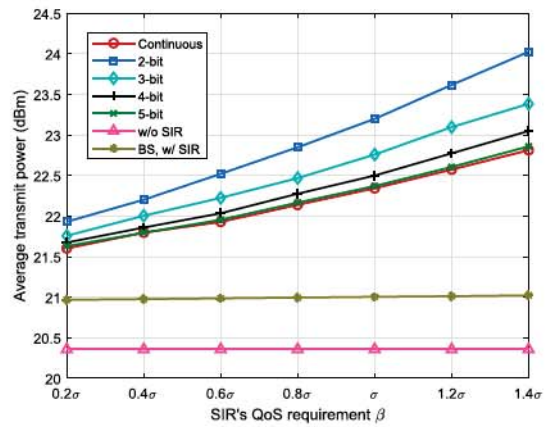

Fig. 8. Average transmit power versus SIR's QoS requirement β ($K = 3$, $N = 100$, $\alpha = 2.5\sigma$).

B. Joint Passive Reflection and Information Transmission System

In this subsection, we present simulation results for the joint passive reflection and information transmission designs in Sec. III. We assume that the BS is equipped with $M = 6$ antennas and serves $K = 3$ PIRs and one SIR. Since the IRS is usually deployed near the BS or users to achieve more beamforming gains, we assume that the IRS is 10 m away from the BS, the PIRs are 100 m away from the IRS, and the SIR is 20 m away from the IRS to facilitate the secondary information transmission. Since the BS and IRS are usually deployed at higher elevation to avoid undesired blockages, we assume that the channel between the BS and IRS is stronger than the others. In particular, the BS-IRS channel is assumed to follow a small-scale Rician fading model with LoS and NLoS components whose path-loss exponent is 2.5, while the other channels only have NLoS components and with a path-loss exponent of 3. For simplicity, we assume that the QoS requirements and weight coefficients for the PIRs are the same, i.e., $\alpha_k = \alpha$, $\rho_k = \rho = 1$, $\forall k$, and the weight coefficient for the SIR is $\varrho = 5$.

The simulation results for the power minimization problem are shown in Figs. 6– 8. We first demonstrate the convergence performance in Fig. 6, where the average transmit power versus the number of iterations is plotted. It shows that the convergence can be achieved within 20 iterations, which demonstrates a reasonable computational complexity. Furthermore, we observe that the low-resolution cases have faster convergence than the continuous counterpart. As in Fig. 4, 1-bit phase-shifts show a notable performance loss due to the quantization error and thus will not be evaluated in the rest of the simulation studies.

Fig. 7 shows the average transmit power versus the PIR QoS requirement α with fixed SIR QoS requirement $\beta = 0.5\sigma$. For comparison, we also show the performance for the case where there is no SIR and the IRS only works as a passive reflector for enhancing the primary information transmissions. These results are plotted as a benchmark and denoted by "w/o SIR". We also consider the scheme where the IRS transfers the secondary information to the BS and the BS simultaneously serves the PIRs and SIR with the aid of the IRS. This case is denoted as "BS, w/ SIR". The "w/o SIR" scheme naturally consumes the least power since it only serves the PIRs. The "BS, w/ SIR" scheme also consumes less power than the proposed schemes due to the BS's powerful processing ability. However, for this case, the IRS must transfer secondary information to the BS, which requires additional power consumption at the IRS and a higher

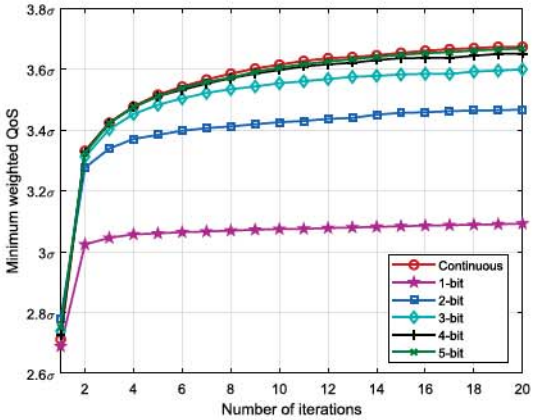

Fig. 9. Minimum weighted QoS versus the number of iterations ($K = 3, N = 100$, $P = 25$dBm).

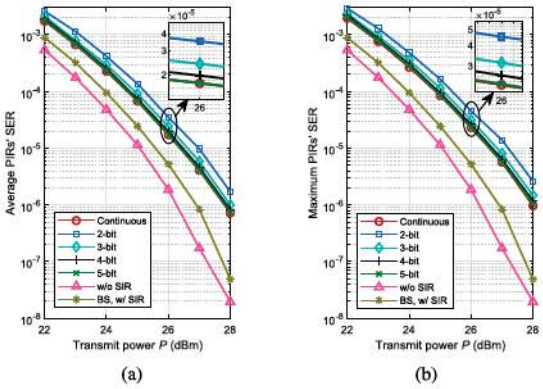

Fig. 10. SER versus average transmit power P ($K = 3, N = 100$). (a) Average SER versus P. (b) Maximum SER versus P.

transmission bandwidth for the control link between the BS and IRS. Moreover, compared with the case where there is no SIR, less than 1.5 dBm extra power is required, which shows the effectiveness of the proposed scheme. Since the symbol-level precoding at the BS provides significant additional DoFs, the performance loss due to quantization of the IRS phases is much lower in this scenario compared with that in Fig. 4.

In Fig. 8, we plot the average transmit power versus the SIR QoS requirement β with fixed PIR QoS requirement $\alpha = 2.5\sigma$. We see that as β increases, only a small amount of extra power is required to provide better QoS for the SIR, especially for the high-resolution cases, which illustrates the effectiveness of our proposed scheme for embedding the secondary symbols into primary transmissions.

Figs. 9– 11 show simulation results for the QoS balancing problem. In Fig. 9, the minimum weighted QoS versus the number of iterations is plotted to show the convergence of the proposed algorithm. As in the previous examples, convergence is faster for the low-resolution cases, but in all cases it is achieved relatively quickly, within about 20 iterations, although little performance improvement is observed beyond about 10 iterations.

In Fig. 10, the average and maximum PIR SER versus transmit power P are plotted to show the QoS balancing performance.

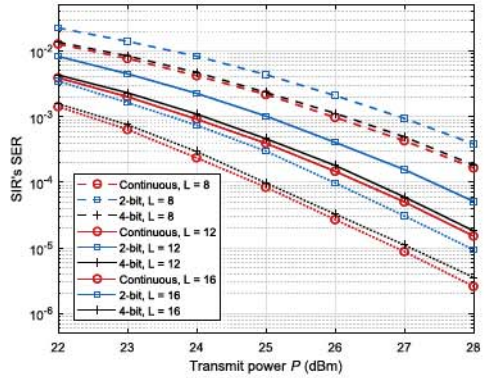

Fig. 11. Average SER of SIR versus average transmit power P ($K = 3, N = 100$).

We observe that the performance gap between Fig. 10(a) and Fig. 10(b) is relatively small, which fits well with the setting $\rho_k = 1, \forall k$. In addition, comparing the "BS, w/ SIR" and "w/o SIR" schemes, the performance loss of the proposed continuous approach is about 1 dBm and 1.5 dBm, respectively, which is a reasonable cost for transmitting the additional secondary information. Moreover, the efficient low-resolution schemes also have encouraging performance.

The SIR SER versus transmit power P is shown in Fig. 11, including continuous, 2-bit, and 3-bit phase resolution with different embedding rates, $L = 8, 12, 16$. We observe that SER decreases with increasing L, revealing the trade-off between efficiency and reliability.

V. Conclusion

In this paper, we investigated IRS-assisted passive information transmissions in downlink MU-MISO systems by exploiting symbol-level precoding. A dedicated passive information transmission system was first considered, where the IRS operates as a passive transmitter by reflecting an unmodulated carrier signal from an RF generator to multiple users. Then, a joint passive reflection and information transmission system was investigated, where the IRS enhances primary information transmissions and simultaneously delivers its own secondary information. Efficient algorithms were proposed to solve the power minimization and QoS balancing problems for both systems. Extensive simulation results confirmed the feasibility of IRS-assisted passive information transmission and the effectiveness of the proposed algorithms.

References

[1] S. Zhang, Q. Wu, S. Xu, and G. Y. Li, "Fundamental green tradeoffs: Progress, challenges, and impacts on 5 G networks," *IEEE Commun. Surv. Tut.*, vol. 19, no. 1, pp. 33–56, Jan.–Mar. 2017.

[2] C. Liaskos, S. Nie, A. Tsioliaridou, A. Pitsillides, S. Ioannidis, and I. Akyildiz, "A new wireless communication paradigm through software-controlled metasurfaces," *IEEE Commun. Mag.*, vol. 56, no. 9, pp. 162–169, Sep. 2018.

[3] E. Basar, M. D. Renzo, J. Rosny, M. Debbah, M.-S. Alouini, and R. Zhang, "Wireless communications through reconfigurable intelligent surfaces," *IEEE Access*, vol. 7, pp. 116753–116773, Aug. 2019.

[4] E. Björnson, L. Sanguinetti, H. Wymeersch, J. Hoydis, and T. L. Marzetta, "Massive MIMO is a reality-What is next?: Five promising research directions for antenna arrays," *Digit. Signal Process.*, vol. 94, pp. 3–20, Nov. 2019.

[5] M. D. Renzo *et al.*, "Smart radio environments empowered by reconfigurable intelligent surfaces: How it works, state of research, and the road ahead," *IEEE J. Sel. Areas Commun.*, vol. 38, no. 11, pp. 2450–2525, Nov. 2020.

[6] S. Gong *et al.*, "Towards smart wireless communications via intelligent reflecting surfaces: A contemporary survey," *IEEE Commun. Surv. Tut.*, vol. 22, no. 4, pp. 2283–2314, Oct.–Dec. 2020.

[7] Q. Wu and R. Zhang, "Towards smart and reconfigurable environment: Intelligent reflecting surface aided wireless network," *IEEE Commun. Mag.*, vol. 58, no. 1, pp. 106–112, Jan. 2020.

[8] Q. Wu, S. Zhang, B. Zheng, C. You, and R. Zhang, "Intelligent reflecting surface aided wireless communications: A tutorial," *IEEE Trans. Commun.*, vol. 69, no. 5, pp. 3313–3351, May 2021.

[9] N. Shlezinger, G. C. Alexandropoulos, M. F. Imani, Y. C. Eldar, and D. R. Smith, "Dynamic metasurface antennas for 6 G extreme massive MIMO communications," *IEEE Wireless Commun.*, vol. 28, no. 2, pp. 106–113, Apr. 2021.

[10] Q. Wu and R. Zhang, "Intelligent reflecting surface enhanced wireless network via joint active and passive beamforming," *IEEE Trans. Wireless Commun.*, vol. 18, no. 11, pp. 5394–5409, Nov. 2019.

[11] R. Liu, M. Li, Q. Liu, and A. L. Swindlehurst, "Joint symbol-level precoding and reflecting designs for IRS-enhanced MU-MISO systems," *IEEE Trans. Wireless Commun.*, vol. 20, no. 2, pp. 798–811, Feb. 2021.

[12] A. Zappone, M. D. Renzo, F. Shams, X. Qian, and M. Debbah, "Overhead-aware design of reconfigurable intelligent surfaces in samrt radio environments," *IEEE Trans. Wireless Commun.*, vol. 20, no. 1, pp. 126–141, Jan. 2021.

[13] C. Huang, A. Zappone, G. C. Alexandropoulos, M. Debbah, and C. Yuen, "Reconfigurable intelligent surfaces for energy efficiency in wireless communication," *IEEE Trans. Wireless Commun.*, vol. 18, no. 8, pp. 4157–4170, Aug. 2019.

[14] N. S. Perović, M. D. Renzo, and M. F. Flanagan, "Channel capacity optimization using reconfigurable intelligent surfaces in indoor mmWave environments," in *Proc. IEEE Int. Conf. Commun.*, Dublin, Ireland, Jun. 2020, pp. 1–7.

[15] C. Pan *et al.*, "Multicell MIMO communications relying on intelligent reflecting surface," *IEEE Trans. Wireless Commun.*, vol. 19, no. 8, pp. 5218–5233, Aug. 2020.

[16] J. Ye, S. Guo, and M.-S. Alouini, "Joint reflecting and precoding designs for SER minimization in reconfigurable intelligent surfaces assisted MIMO systems," *IEEE Trans. Wireless Commun.*, vol. 19, no. 8, pp. 5561–5574, Aug. 2020.

[17] Y. Liu, J. Zhao, M. Li, and Q. Wu, "Intelligent reflecting surface aided MISO uplink communication network: Feasibility and power minimization for perfect and imperfect CSI," *IEEE Trans. Commun.*, vol. 69, no. 3, pp. 1975–1989, Mar. 2021.

[18] X. Yu, D. Xu, Y. Sun, D. W. K. Ng, and R. Schober, "Robust and secure wireless communications via intelligent reflecting surfaces," *IEEE J. Sel. Areas Commun.*, vol. 38, no. 11, pp. 2637–2652, Nov. 2020.

[19] C. Huang, R. Mo, and C. Yuen, "Reconfigurable intelligent surface assisted multiuser MISO systems exploiting deep reinforcement learning," *IEEE J. Sel. Areas Commun.*, vol. 38, no. 8, pp. 1839–1850, Aug. 2020.

[20] H. Yang, Z. Xiong, J. Zhao, D. Niyato, L. Xiao and Q. Wu, "Deep reinforcement learning-based intelligent reflecting surface for secure wireless communications," *IEEE Trans. Wireless Commun.*, vol. 20, no. 1, pp. 375–388, Jan. 2021.

[21] C. Huang *et al.*, "Holographic MIMO surfaces for 6 G wireless networks: Opportunities, challenges, and trends," *IEEE Wireless Commun.*, vol. 27, no. 5, pp. 118–125, Oct. 2020.

[22] Z. Wan, Z. Gao, F. Gao, M. D. Renzo, and M.-S. Alouini, "Terahertz massive MIMO with holographic reconfigurable intelligent surfaces," *IEEE Trans. Commun.*, vol. 69, no. 7, pp. 4732–4750, Jul. 2021.

[23] W. Tang *et al.*, "Wireless communications with programmable metasurface: Transceiver design and experimental results," *China Commun.*, vol. 16, no. 5, pp. 46–61, May 2019.

[24] W. Tang *et al.*, "Programmable metasurface-based RF chain-free 8PSK wireless transmitter," *Electron. Lett.*, vol. 55, no. 7, pp. 417–420, Apr. 2019.

[25] N. V. Huynh, D. T. Hoang, X. Lu, D. Niyato, P. Wang, and D. I. Kim, "Ambient backscatter communications: A contemporary survey," *IEEE Commun. Surv. Tut.*, vol. 20, no. 4, pp. 2889–2992, Oct.–Dec. 2018.

[26] Y.-C. Liang, Q. Zhang, E. G. Larsson, and G. Y. Li, "Symbiotic radio: Cognitive backscattering communications for future wireless networks," *IEEE Trans. Cogn. Commun. Netw.*, vol. 6, no. 4, pp. 1242–1255, Dec. 2020.

[27] W. Yan, X. Kuai, and X. Yuan, "Passive beamforming and information transfer via large intelligent surface," *IEEE Wireless Commun. Lett.*, vol. 9, no. 4, pp. 533–537, Apr. 2020.

[28] W. Yan, X. Yuan, Z.-Q. He, and X. Kuai, "Passive beamforming and information transfer design for reconfigurable intelligent surfaces aided multiuser MIMO systems," *IEEE J. Sel. Areas Commun.*, vol. 38, no. 8, pp. 1793–1808, Jun. 2020.

[29] S. Guo, S. Lv, H. Zhang, J. Ye, and P. Zhang, "Reflecting modulation," *IEEE J. Sel. Areas Commun.*, vol. 38, no. 11, pp. 2548–2561, Nov. 2020.

[30] Q. Zhang, Y.-C. Liang, and H. V. Poor, "Large intelligent surface/antennas (LISA) assisted symbiotic radio for IoT communications," Feb. 2020. [Online]. Available: https://arxiv.org/abs/2002.00340

[31] E. Basar, "Reconfigurable intelligent surface-based index modulation: A new beyond MIMO paradigm for 6 G," *IEEE Trans. Commun.*, vol. 68, no. 5, pp. 3187–3196, May 2020.

[32] Y. Ma, R. Liu, M. Li, and Q. Liu, "Passive information transmission in intelligent reflecting surface aided MISO systems," *IEEE Commun. Letts.*, vol. 24, no. 12, pp. 2951–2955, Dec. 2020.

[33] C. Masouros and G. Zheng, "Exploiting known interference as green signal power for downlink beamforming optimization," *IEEE Trans. Signal Process.*, vol. 63, no. 14, pp. 3628–3640, Jul. 2015.

[34] A. Li and C. Masouros, "Interference exploitation precoding made practical: Optimal closed-form solutions for PSK modulations," *IEEE Trans. Wireless Commun.*, vol. 17, no. 11, pp. 7661–7676, Nov. 2018.

[35] P. Amadori and C. Masouros, "Constant envelope precoding by interference exploitation in phase shift keying-modulated multiuser transmission," *IEEE Trans. Wireless Commun.*, vol. 16, no. 1, pp. 538–550, Jan. 2017.

[36] F. Liu, C. Masouros, P. V. Amadori, and H. Sun, "An efficient manifold algorithm for constructive interference based constant envelope precoding," *IEEE Signal Process. Lett.*, vol. 24, no. 10, pp. 1542–1546, Sep. 2017.

[37] M. A. Sedaghat, V. I. Barousis, R. R. Müller, and C. B. Papadias, "Load modualted arrays: A low-complexity antenna," *IEEE Commun. Mag.*, vol. 54, no. 3, pp. 46–52, Mar. 2016.

[38] C. You, B. Zheng, and R. Zhang, "Channel estimation and passive beamforming for intelligent reflecting surface: Discrete phase shift and progressive refinement," *IEEE J. Sel. Areas Commun.*, vol. 38, no. 11, pp. 2604–2620, Nov. 2020.

[39] B. Zheng, C. You, and R. Zhang, "Intelligent reflecting surface assisted multi-user OFDMA: Channel estimation and training design," *IEEE Trans. Wireless Commun.*, vol. 19, no. 12, pp. 8315–8329, Dec. 2020.

[40] G. T. D. Araujo, A. L. F. D. Almeida, and R. Boyer, "Channel estimation for intelligent reflecting surface assisted MIMO systems: A tensor modeling approach," *IEEE J. Sel. Topics Signal Process.*, vol. 15, no. 3, pp. 789–802, Apr. 2021.

[41] L. Wei, C. Huang, G. C. Alexandropoulos, C. Yuen, Z. Zhang, and M. Debbah, "Channel estimation for RIS-empowered multi-user MISO wireless communications," *IEEE Trans. Commun.*, vol. 69, no. 6, pp. 4144–4157, Jun. 2021.

[42] X. Guan, Q. Wu, and R. Zhang, "Anchor-Assisted Intelligent Reflecting Surface Channel Estimation for Multiuser Communications," Feb. 2021. [Online]. Available: https://arxiv.org/abs/2102.10886

[43] P.-A. Absil, R. Mahony, and R. Sepulchre, *Optimization Algorithms on Matrix Manifolds*. Princeton, NJ, USA: Princeton Univ. Press, 2009.

[44] Q. Wu and R. Zhang, "Beamforming optimization for wireless network aided by intelligent reflecting surface with discrete phase shifts," *IEEE Trans. Commun.*, vol. 68, no. 3, pp. 1838–1851, Mar. 2020.

[45] P. M. Narendra and K. Fukunaga, "A branch and bound algorithm for feature subset selection," *IEEE Trans. Comput.*, vol. 26, no. 9, pp. 917–922, Sep. 1977.

Rang Liu (Graduate Student Member, IEEE) received the B.S. degree in 2018 in electronics information engineering from the Dalian University of Technology, Dalian, China, where she is currently working toward the Ph.D. degree with the School of Information and Communication Engineering. Her current research interests include signal processing, mmWave communications, massive MIMO systems, and reconfigurable intelligent surfaces.

Ming Li (Senior Member, IEEE) received the M.S. and Ph.D. degrees in electrical engineering from the State University of New York at Buffalo (SUNY-Buffalo), Buffalo, NY, USA, in 2005 and 2010, respectively. From January 2011 to August 2013, he was a Postdoctoral Research Associate with the Department of Electrical Engineering, SUNY-Buffalo. From August 2013 to June 2014, he joined Qualcomm Technologies Inc., San Diego, CA, USA, as a Senior Engineer. Since June 2014, he has been with the School of Information and Communication Engineering, Dalian University of Technology, Dalian, China, where he is currently a Professor. His current research interests include communication theory and signal processing with applications to intelligent reflecting surface, mmWave communications, massive MIMO systems, and secure wireless communications. He is the Co-Chair for IEEE INFOCOM 2019 workshop on *Wireless Communications and Networking in Extreme Environments*.

Qian Liu (Member, IEEE) received the B.S. and M.S. degrees the from the Dalian University of Technology, Dalian, China, in 2006 and 2009, respectively, and the Ph.D. degree from The State University of New York at Buffalo (SUNY-Buffalo), Buffalo, NY, USA, in 2013. From 2013 to 2015, she was a Postdoctoral Fellow with Ubiquitous Multimedia Laboratory, SUNY-Buffalo. From 2016 to 2017, she was a Postdoctoral Fellow with the Chair of Media Technology and the Chair of Communication Networks, Technical University of Munich, Munich, Germany. She is currently an Associate Professor with the School of Computer Science and Technology, Dalian University of Technology. Her current research interests include multimedia transmission over MIMO systems, IEEE 802.11 wireless networks and LTE networks, device-to-device communication, energy-aware multimedia delivery, and tactile Internet. She was the recipient of the Best Paper Runner-up Award at the 2012 IEEE International Conference on Multimedia and Expo and was in the finalist for the Best Student Paper Award at the 2011 IEEE International Symposium on Circuits and Systems. She was also the recipient of the Alexander von Humboldt Fellowship in 2015.

A. Lee Swindlehurst (Fellow, IEEE) received the B.S. and M.S. degrees in electrical engineering from Brigham Young University (BYU), Provo, UT, USA, in 1985 and 1986, respectively, and the Ph.D. degree in electrical engineering from Stanford University, Stanford, CA, USA, in 1991. From 1990 to 2007, he was with the Department of Electrical and Computer Engineering, BYU, where he was the Department Chair from 2003 to 2006. During 1996–1997, he held a joint appointment as a Visiting Scholar with the Uppsala University, Uppsala, Sweden and the Royal Institute of Technology, Stockholm, Sweden. From 2006 to 2007, he was on leave as the Vice President of Research for ArrayComm LLC, San Jose, CA, USA. Since 2007, he has been a Professor with the Electrical Engineering and Computer Science Department, University of California Irvine, Irvine, CA, USA, where he was the Associate Dean for Research and Graduate Studies with the Samueli School of Engineering from 2013 to 2016. During 2014–17, he was also a Hans Fischer Senior Fellow with the Institute for Advanced Studies, Technical University of Munich, Munich, Germany. In 2016, he was elected as a Foreign Member of the Royal Swedish Academy of Engineering Sciences. He has more than 300 publications in his research field, which include array signal processing for radar, wireless communications, and biomedical applications. He was the inaugural Editor-in-Chief of the IEEE JOURNAL OF SELECTED TOPICS IN SIGNAL PROCESSING. He was the recipient of the 2000 IEEE W. R. G. Baker Prize Paper Award, the 2006 IEEE Communications Society Stephen O. Rice Prize in the field of communication theory, the 2006 and 2010 IEEE Signal Processing Society's Best Paper Awards, and the 2017 IEEE Signal Processing Society Donald G. Fink Overview Paper Award.

Qingqing Wu (Member, IEEE) received the B.Eng. degree in electronic engineering from the South China University of Technology, Guangzhou, China, in 2012 and the Ph.D. degree in electronic engineering from Shanghai Jiao Tong University (SJTU), Shanghai, China, in 2016. He is currently an Assistant Professor with the State key laboratory of Internet of Things for Smart City, University of Macau, Macau. From 2016 to 2020, he was a Research Fellow with the Department of Electrical and Computer Engineering, National University of Singapore, Singapore. His current research interests include intelligent reflecting surface, unmanned aerial vehicle (UAV) communications, and MIMO transceiver design.

He was the recipient of the IEEE Communications Society Young Author Best Paper Award in 2021, the Outstanding Ph.D. Thesis Award of China Institute of Communications in 2017, the Outstanding Ph.D. Thesis Funding in SJTU in 2016, and the IEEE WCSP Best Paper Award in 2015. He was the Exemplary Editor of the IEEE COMMUNICATIONS LETTERS in 2019 and the Exemplary Reviewer of several IEEE journals. He is an Associate Editor for the IEEE COMMUNICATIONS LETTERS, IEEE WIRELESS COMMUNICATIONS LETTERS, IEEE OPEN JOURNAL OF COMMUNICATIONS SOCIETY, and IEEE OPEN JOURNAL OF VEHICULAR TECHNOLOGY. He is the Lead Guest Editor of the IEEE JOURNAL ON SELECTED AREAS IN COMMUNICATIONS on UAV Communications in 5G and Beyond Networks, and the Guest Editor for the IEEE OPEN JOURNAL OF VEHICULAR TECHNOLOGY on 6G Intelligent Communications and IEEE OPEN JOURNAL OF COMMUNICATIONS SOCIETY on Reconfigurable Intelligent Surface-Based Communications for 6G Wireless Networks. He is the workshop Co-Chair of the IEEE ICC 2019-2021 workshop on Integrating UAVs into 5G and Beyond, and the workshop Co-Chair of the IEEE GLOBECOM 2020 and ICC 2021 workshop on Reconfigurable Intelligent Surfaces for Wireless Communication for Beyond 5G. He is the Workshops and Symposia Officer of Reconfigurable Intelligent Surfaces Emerging Technology Initiative and Research Blog Officer of Aerial Communications Emerging Technology Initiative. He is the IEEE ComSoc Young Professional Chair in APB. He was listed as a Worlds Top 2% Scientist by Stanford University, Stanford, CA, USA, in 2020.